UNIVERSITY OF STRATHCLYDE

FACULTY OF ENGINEERING BIOENGINEERING UNIT

PROPERTY DETERMINATION OF BIOMEDICAL POLYMER SCAFFOLDS FOR CERVICAL TISSUE REPAIR

NADIRA ABDI SALAH

A DISSERTATION SUBMITTED IN PARTIAL FULFILMENT OF THE REQUIREMENTS OF THE AWARD OF MASTERS OF SCIENCE IN BIOMEDICAL ENGINEERING

Declaration of Authenticity

This thesis is the result of the author's original research. It has been composed by the author and has not been previously submitted for examination, which has led to the award of a degree.

Signed: ..... Date: ..... / ..... / 2014

Abstract

Cervical cancer is the second most common cancer disease among women and around 1/2 million women are diagnosed each year. Treatment options include surgery, such as hysterectomy, or radiotherapy. Both treatments make childbearing impossible. Other well-known medical issues related to the uterine cervix (UC) are insufficiency and abnormality of the cervix, which causes preterm childbirth. The UC is a cylindrical shaped narrow part of the uterus and connects the uterus to the vagina. It varies in size, thickness and shape depending on age, menstrual cycle and pregnancy.

This study aims to design and investigate the mechanical properties of a nano-scaled polymer scaffold based on the porcine uterine cervix (PUC).
The permeability and mechanical properties of electrospunned polyurethane scaffolds of two different polymer grades, Z1A1 and Z3A1, were investigated in order to explore the possibilities of applying these scaffolds in the future for tissue engineered UC.
Methods of evaluation of this study were permeability testing, stress-relaxation test, dynamic mechanical analysis (DMA) as well as scanning electron microscopy (SEM). The Z1A1 and Z3A1 samples were tested with and without impregnation of gelatine hydrogels in order to mimic tissue formation.
The permeability of the Z3A1 scaffolds was found to be significantly higher than Z1A1 scaffolds when compared. The stress relaxation test showed that a higher stress was needed in order to elongate the Z3A1 samples in air, which indicates that these samples had a lower elasticity compared to Z1A1 samples tested in air. This difference in elasticity was also confirmed in the hysteresis test in air, which showed that the Z3A1 samples were stiffer when compared to the Z1A1 samples.
The results for the gelatine impregnated samples in both the hysteresis test as well as the stress relaxation test showed that there was no consistency in the mechanical properties of the samples when they were compared to the samples without gelatine

impregnation and between Z1A1 and Z3A1 impregnated samples. This inconstancy was especially shown when samples were compared at different strain levels.

Acknowledgements

First and foremost I would like to give my sincere gratitude to my supervisor Dr. Richard A. Black, for who has supported and advised me throughout my thesis. His expertise, knowledge, patience and advice were greatly valued as well as allowing me to do my own work.

I would like to express my great appreciation to Milovan J. Cardona and Davide Erbogasto for providing the Z1A1 and Z3A1 electrospun scaffolds as well as guidance, knowledge and technical assistance during this thesis.
I would also like to thank Supraja Suresh for her much appreciated guidance and instructions on the various test procedures applied in this thesis. I want thank Katie Henderson for her technical assistance and guidance.

Lastly, I would like to express my sincere gratitude to my family and especially my parents for their love, support and always being there, when I needed them.

Table of Contents

List of Figures

List of Tables

List of Abbreviations

DMA - Dynamic Mechanical Analysis

DMF - Dimethylformamide

ECM – Extracellular matrix

LS – Longitudinal samples without gelatine impregnation

LSG – Longitudinal samples with gelatine impregnation

PCL – Polycaprolactone

PGA - Poly(glycolic acid)

PUC - Porcine uterine cervix

PLGA – Poly(lactic-co-glycolic acid)

PLLA - Poly(lactic acid)

RS – Ring-shaped samples without gelatine impregnation

RSG – Ring-shaped samples with gelatine impregnation

SEM – Scanning Microscopy Electron

THF - Tetrahydrofuran (THF)

UC – Uterine cervix

1. Introduction

Cervical cancer is the second most common cancer disease among women and around 1/2 million women are diagnosed each year. Treatment options include surgery, such as hysterectomy, or radiotherapy. Both treatments make childbearing impossible [1]. The functions of the uterine cervix (UC) have a great impact on the outcome of a pregnancy. A diminished cervical function can lead to well-known clinical complications such as cervical insufficiency, which results in pre-term childbirth due to premature dilation of the cervix. The differing, where there is absence of cervical dilation during parturition also occurs and can result in severe morbidity of both the mother and the foetus [2].

This study aims to design and investigate the mechanical properties of a nano-scaled polyurethane scaffolds in order to explore the possibilities of applying these scaffolds for repairing cervical tissue in the future and to overcome the above-described pathologies of the UC.
However this project is the first approach in the step towards determining a polymer scaffold for a possible cervical tissue repair and therefor the project only investigates the mechanical properties, such as the viscoelastic behaviour and the permeability of the electrospun polyurethane scaffolds in order to determine if these scaffolds are valuable for cervical tissue repair.

2. Literature Review

2.1 Introduction

2.1.1 The Human Uterine Cervix

The human UC is a narrow part of the uterus that connects the uterus to the vaginal canal. Depending on age, menstrual cycle and pregnancy it varies in size, thickness and shape. The UC is typically cylindrical shaped with an approximately diameter of 2 to 2.5 cm and a length of 3 to 4 cm in which 1.25 cm of it projects into the vaginal canal [4]. During parturition the UC is very extensible and dilates to 10 cm in diameter but it also posses a reversible extensibility as it has a shape-recovering process after childbirth [5].

2.1.2 Pathology

Cervical cancer is one of the severest cervical diseases and is the most common cancer among young women in the age of 15-34 years. 16% of all diagnosed cancer in the UK is cervical cancer [6] and each year 38,000 women are diagnosed with cervical cancer while more than 350,000 women diagnosed dies worldwide [1]. Cervical cancer occurs due to abnormal and excessive cell growth in the UC resulting in malign tumour formation [6].

Another well-known cervical morbidity is insufficiency and abnormalities of the UC; such as shorten of the UC, which in must cases results in premature or absence of cervical dilation. If not treated this can lead to high maternal and neonatal mortality and morbidity [7].

A screening study at 22 to 24 weeks, carried out by Heath et al., has shown that a decrease in cervical length implicated in an increase for premature parturition.

Table 1 shows the relationship between different cervical lengths in week 22 to 24 and the risk of preterm birth [8].

Cervical Length (mm)	Risk of Preterm Birth (%)
60	0.2
25	1.1
15	4.0
5	78

Table 1. Relationship between cervical length and risk of preterm birth

Preterm parturition is defined as childbirth before 37 weeks and is the only main cause in neonatal mortality and is accountable for 50 % of all neonatal mortalities. The mortality rate increases as the time of gestation decreases, rising from 2% at gestation at 32 weeks to more than 90% at 23 weeks and moreover, the disability also increases for premature neonates [9]. The health service costs associated with this issue are enormous due to the need for prolonged intensive neonatal care and continuous aftercare upon discharge from hospital [10]. Cervical cerclage has been applied for treating and minimizing the risk of premature parturition. This surgical procedure involves suturing a cerclage around the UC in order to prevent premature cervical dilation.

Meeka et al. have carried out a randomized controlled trial study in order to investigate if the use of cervical cerclage implicated a reduction of premature delivery. The study was performed with more than 45,000 pregnancies throughout 12 different clinics in UK, Brazil, South Africa, Slovenia, Greece, and Chile. They concluded that there was no significant decrease in premature delivery when cervical cerclage was applied, although previous studies have implied this is indeed the case [11].

2.1.3 Tissue Engineering of The Female Reproductive System

Numerous of studies have investigated the development of female reproductive specific cells, tissues, and organs for clinical application. Some of these include engineering a functional uterine tissue using autologous cells, reconstruction of a three-dimensional cervical tissue, and engineering vaginal tissue in vivo [12,13,14].

A possible approach to overcome premature birth due to cervical morbidity is to reconstruct a tissue engineered UC. House et al. have studied the possibility of reconstructing a three-dimensional cervical tissue by using collagen coated porous silk scaffolds. Cervical fibroblasts were harvested from pre-menopausal women and seeded on the scaffolds. After eight weeks of cell culturing the cells proliferated in the scaffold and an extracellular matrix similar to native tissue was created. The silk scaffolds were preferred due to the capability of controlling the morphology and the functional and mechanical properties of the scaffolds as these scaffold's pore size can be easily controlled. Solvent Casting/ Particular leaching was applied as scaffold fabrication method for the porous silk scaffolds. Silk was retrieved from coccons of the Bombyx mori silk-worm and treated in boiled aqueous solution producing purified silk fibroin protein, which afterwards was processed into rectangular silk sponges. In order to enhance cell proliferation the scaffolds were coated with collagen as previous studies have showed poor cell proliferation on silk surfaces [14].

2.2 The Pig as a Model Organism for Biomedical Research

The pig has become increasingly favoured as model organism in biomedical research, as the anatomy, physiology and genetics shows some resembling to those of humans. This is especially true in the early reproductive stages. The average length of the pig oestrous cycle and hormonal characteristics suggest that its hormonal regulation of cyclic events follow the same principles as the human. The pattern of sperm transport within the upper part of the abdomen of the pig also has the same characteristics as human [3, 15,16,17,18]. This makes the pig one of the most interesting model organisms for reproductive research with regard to the possible application of the

results to human physiology [19]. Besides the resembling in biology, pigs are also easy to breed and it is easy to retrieve biopsies and post-mortem samples. Miniature pigs are preferred in most biomedical researches, due to their low grow rate compared to large farm breeds. A large growth rate can give rise to complications for the research (such as ergonomic injuries) but also induce potential health hazard [3,20].

2.3 Porcine Uterine Cervix

2.3.1 Anatomy and Physiology

The PUC is a part of the uterus and connects the uterus to the vagina. It is typically cylindrical shaped and varies in size, thickness and shape depending on age, menstrual cycle and pregnancy. The PUC is very extensible and dilates during parturition. Although studies of porcine cervical dilation is limited, Kertiles et al. investigated the effect of relaxin on cervical dilation and their experiment showed cervical dilation up to 50.8 mm [21]. The UC posses a reversible extensibility as it has a shape-recovering process after parturition [22].

The PUC can be divided in two parts: a long vaginal portion and the uterine portion. The vaginal-cervical transition is continuous, which makes it difficult to determine the distinct end of the cervix, whereas the utero-cervical transition is more apparent [23,24].

This study will mainly focus on the uterine portion of the UC, as this portion has similar anatomical and morphological characteristics as the human UC.

The UC has a typical morphology similar to a tubular organ and has four major layers: the mucosa, the submucosa, muscular layer, and tunica externa. The inner lining, mucosa, consists of epithelium, which is composed with ciliated cells and lamina properia, which consists of a thin layer of connective tissue. The submucosa mainly consists loose connective tissue with numerous collagen fibres, fibroblasts, glandular epithelia and high proportion of blood vessels compared with the vaginal cervix. The muscular layer can be divided into two parts: 1) the internal muscular

layer, which consists of circular smooth muscles and 2) the external muscular layer, which consist of longitudinal smooth muscles. The tunica externa consists mostly of dense connective tissue [25].

2.3.2 Dimensions of the uterine portion of the UC

The uterine portion of the PUC is 4-5cm in length and approximately 2.5-3.0cm in diameter. The thickness of the UC wall is usually between 3.035-3.273mm. The thickness of the wall is influenced by the oestrous cycle due to changes of the height of the epithelial cells, which can vary between 26.0-28.8μm (at day 5-9 of the oestrus cycle) and 40.1-58.3μm (at day 21-22 of the oestrus cycle) [26].

Based on the above, the desired polymer scaffold in this study is a nano-scaled polyurethane scaffold that mimics the structure of the uterine portion of the porcine UC.

2.4 Mechanical Properties of the Uterine Cervix

A number of studies have investigated the mechanical properties of the UC and they have shown that the mechanical properties of the cervical tissue depends on the biochemical characteristics, the obstetric history, the anatomical site in which the samples are taken from, and on the direction in which the load is applied as the UC is an anisotropic tissue.

Conrad et al. have in their study presented a significantly larger stiffness of cervical tissue from non-pregnant specimens compared to cervical tissue from pregnant specimens [27]. This was further explained in the study carried out by Rechberger et al. as they stated that there was a relationship between the increase in collagen, reduction in sulfated glycosaminoglycans, an increase in hydration in pregnant specimens and a decrease in the mechanical strength. They also reported a relationship between the mechanical properties and the direction in which the tensile

load was applied, showing that an elongation of the specimens in the longitudinal direction showed a higher creep rate than when elongated in the circumferential direction [28].

Meyers et al. investigated the mechanical properties of the human UC in order to determine the anisotropic response of the tissue when undergoing compression and tension. Samples were taken from two cervix types from pre-menopausal women who underwent hysterectomy. Compressive and tension mechanical tests were performed on cervical tissue with three different obstetric history: Non-pregnant with no previous vaginal delivery (NPND), Non-pregnant with previous vaginal delivery (NPPD), and pregnant women with cesarean delivery (PCS). Cylindrical samples were applied for the compressive tests, as compression loads usually occur in the longitudinal direction due to the weight of the foetus. The samples for tension testing were ring-shaped as the resistance in the circumferential direction induces tension. These samples had an inner diameter of 6-8mm and an outer diameter of 16-18mm.

The compressive mechanical tests performed were 1) load-unload cycles 2) confined compression test and 3) unconfined compression test in order to achieve adequate data to analyse and characterise the mechanical behaviour, such as the poroelasticity and viscoelasticity of the cervical tissue. These tests were all performed at a strain rate of 0.1% s^{-1}. According to the study the confined compression tests results in larger volume changes in the tissue while the unconfined compression tests result in larger shear deformation.

The ring-shaped samples for the tensile mechanical tests were elongated along their diameter at a constant strain rate of 0.05 mm s^{-1}. The selected strain rate for the compression test was based on physiological concerns, such as uterine contractions and transient increase in inter-abdominal pressure due e.g. coughing, while the strain rate applied for the tensile tests was based on physiological condition such as the dilation rate of the cervix during parturition.

In the compression load-unload cycles with a constant strain rate, the cervical tissue

showed to have non-linear behaviour with hysteresis. The maximum detected stress levels were around 1.5 kPa for NPND samples, 0.8kPa for NPPD samples, and around 0.2kPa for PCS samples. In the tensile tests the stress levels were much higher and around 100kPa for the NPND and NPPD samples, while the maximum detected stress level for the PCS samples were around 60kPa. In both test types stress relaxation was detected and along with the hysteresis and thus non-linear behaviour the cervical tissue showed to have viscoelastic characteristics [2].

2.5 Tissue Engineering

Tissue engineering and regenerative medicine are merging interdisciplinary fields, which involves biology, engineering and medical science [29]. The aim is to regenerate healthy human tissue in order to provide a functional tissue with the goal of replacing a diseased or damaged tissue [30]. Tissue engineering is a cell-based theory, as the production of a tissue-engineered tissue is achieved by combining cells and biomaterials.

The process involves harvesting healthy cells from a host through biopsy. The cells are then cultured and expanded in order to provide sufficient cell amount. Simultaneous an appropriate scaffold is produced (Figure 1).

The main functions of a scaffold are to 1) support interaction between the biomaterial and the cells, enhance cell adhesion and replace the natural extracellular matrix (ECM), 2) allow transportation of nutrients, gases and regulatory elements in order to increase survival, proliferation and differentiation of cells, 3) degradation of the matrices as tissue regenerates under cell culture, and 4) minimise inflammation and toxicity.

When designing a scaffold the ultimate desired goal is to develop a structure that could mimic and with time eventually replace the natural ECM of the host. The ECM normally serves as a scaffold after injury and enhances tissue repair. It provides mechanical support and regulates cell activities, such as phenotype, genetic expression, development and functions of the cells [29,31].

Scaffolds can in general be derived from natural occurring materials, such as collagen, alignate, chitosan, hyaluronan and fibronectin. These naturally derived materials can be used alone or in combination. The advantages of natural scaffolds are their low toxicity and low inflammatory response upon implantation and have been widely used for in clinical use. On the other hand, characteristics such as strength, controllable degradation rate, porosity and the ability to change shape and size of the synthetic scaffolds are also highly desired and also very reproducible [32]. However, one of the disadvantages of synthetic scaffolds is the absence of cell-recognition signals. The scaffold design can be crucial for not only cell survival but also cell proliferation and growth in order to form a healthy tissue that can replace the damaged tissue [33].

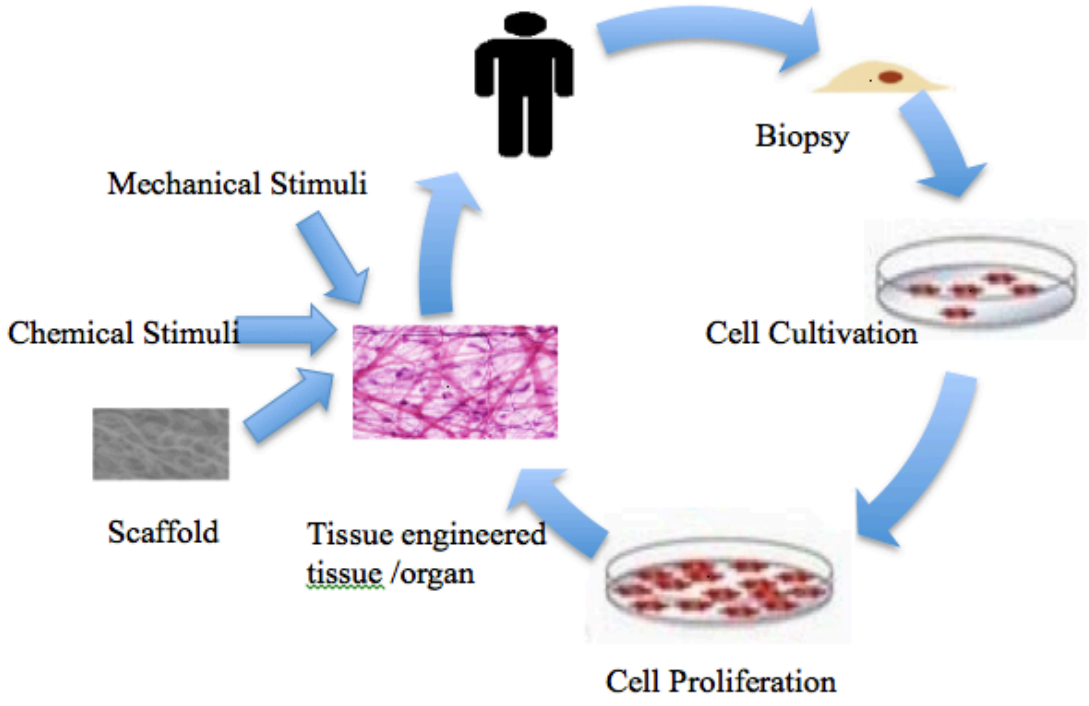

Figure 1. Tissue engineering process

2.6 Polymers for Biomedical Applications

2.6.1 Polymers

Polymers are widely used as biomaterials, due to their ability of being conformable to living tissue and their mechanical and chemical properties. Polymers are extensively used in tissue engineering for scaffold production and they can be biodegradable and non-degradable [33]. In addition, polymers resemble natural derived polymeric tissue components such as collagen. Polymer fibres enhance cell adhesion due to their excellent surface-area-to-volume ratio, making them favourable as biomaterial scaffolds [34].

2.6.1.1 Viscoelastic Behaviour of Polymers

Viscoelasticity is one of the key characteristics of polymers. They exhibit elastic behaviour due their ability to recover after deformation while their viscous behaviour is caused by their ability to creep after a strain.

The viscoelastic characteristics of polymers are highly influenced by the temperature and the viscous or elastic portion of the polymers varies in different temperatures however the viscoelastic properties of the polymers apply at all temperatures. This means that the tensile or elastic modulus depends on the temperature in which the stress is applied and also on the time the stress is applied. Thus the tensile modulus varies with time although keeping the temperature constant.

In general viscoelastic materials are characterised by their ability to creep at constant stress, to relax at constant strain and the occurrence of hysteresis.

Creep deformation appears gradually with prolonged stress, which causes an accumulation of the strain and a rearrangement of the polymer chains. This phenomenon occurs as a result of permanent material deformation in order to release the applied stresses.

Purely elastic materials do not lose energy in the form of heat when stress is applied as these materials have the ability to recover to the original shape. Viscous materials however lose energy due to the materials resistance to plastic deformation when

stress is applied. Hence hysteresis occurs when viscoelastic materials, such as polymers, undergo a loading and unloading cycle. The loss of energy can be observed on a stress-strain curve as the area of the hysteresis loop [35,36].

2.6.2 Polyurethane

Polyurethanes are highly biocompatible and have a wide range of mechanical and biological properties [37], such as processabilty, toughness, durability, surface functionality, flexibility and biostability. This makes polyurethane a favourable and useful biomaterial for drug delivery, tissue engineering, and for various medical devices, such as pacemakers, vascular catheters and grafts, wound healing materials, and for scaffold production in tissue engineering [37,38].

Biodegradable polyurethanes have mechanical properties suitable for soft tissue due to their flexibility, outstanding abrasion and flexural fatigue resistance. Depending on the chemical type, preparation method, and fabrication, polyurethane can be categorised into foams, elastomers or thermoplastics. Polyurethane consists of two segments, a soft segment and a hard segment.

The soft segment consists of long polyester or polyether diol and provides softness and flexibility to the material, while the hard segment operates as a physical cross-linkage between the soft segments and increases the stiffness and changes the toughness of the polymer. The ratio between these two segments defines the elasticity and hardness of the material. An increase of the hard segment content results in an increase of the storage moduli E´ and the glass transition temperature leading to a crystalline material while an increase of the soft segment leads to a more amorphous and therefor a more rubbery material.

In order to have polyurethanes with elastomeric properties they must be 1) above their glass transition temperature; 2) have a very low degree of crystallinity; and 3) lightly cross-linked [39].

Polyurethane can be prepared into a porous scaffold by electrospinning, which is the method that will be applied in this study, or by other methods such as solvent casting / salt leaching, phase inversion, and thermally induced phase separation.

2.6.2.1 b_9 Series 'A' of Medical Grade Polyurethanes

The b_9 Series 'A' of medical grade polyurethanes (Biomer Technology Ltd, Runcorn, Cheshire, UK) have a wide range of mechanical properties, such as their high ultimate tensile strength and ultimate elongation values. This type of polyurethane is therefor ideal for applications that require high flexibility and strength, which is the case in this study. Other properties that characterise the b_9 Series 'A' polyurethanes are [40]:

- Low temperature flexibility
- Wide dynamic range of hardness
- Hydrolytic stability
- Solvent resistance
- Compatible with a wide range of fillers

2.6.3 Hydrogel

Hydrogel is three-dimensional polymeric network that can absorb large quantities of water, 30% or more than its weight. This polymeric material swells extensively due to the water absorption without dissolving the polymeric network and maintaining its dimensional stability. The degree of swelling depends on the interaction with water, the polymer chain flexibility and the density of the crosslinking.

Hydrogels have been applied in many biomedical fields due to their resembling to living tissue, as they allow permeation and diffusion of low molecular weight metabolites, waste products and salts [41,42]. Hydrogels can be classified depending on their preparation methods, ionic charges, sources, nature of swelling with changes in the environment, rate of biodegradation or the nature of crosslinking. Fabrication

methods of hydrogels includes [39]:

- Cast film
- Moulding to produce cross-linked network
- Surface grafting of hydrogel to another polymer
- Interpenetrating polymer network
- Microsphere formation

2.6.3.1 Smart hydrogels

Smart hydrogels are stimuli responsive or environmental sensitive hydrogels that change their swelling nature, polymeric networking, permeability and mechanical strength as a result from environmental changes. These hydrogels can either respond to chemical and biochemical stimuli, such as pH, glucose, proteins and antigens or to physical stimuli, such as temperature, pressure, magnetic and electric field, ultrasound and light [43,44]. Chemical stimuli can change the chemical bonding in the polymers while the physical stimuli influences will affect the level of various energy sources and modify molecular interactions.

2.6.3.2 Hydrogels for Tissue Engineering Scaffolds

Besides being biocompatible, hydrogels have shown to be suitable as scaffolding biomaterial due to their resembling to living tissues and ability to provide an aqueous environment, which simulates those of cells in vivo. Moreover, the porosity of the hydrogels allows diffusion of nutrients and waste product. Synthetic and natural hydrogel scaffolds have been used in previous studies for cartilage, tendon, skin, blood vessels and heart valve repair [45,46].

2.6.3.3 Gelatine Hydrogels

Gelatine is a natural polymer, which can be extracted from animal skin, muscle and bone. It is widely used in tissue engineering due to its biocompatibility, biodegradability and non- immunogenicity. Gelatine is derived from collagen and there are two types of gelatines, gelatine A and gelatine B.

Gelatine A is extracted from collagen by using an acid hydrolysis of collagen and gelatine B is achieved by using an alkaline hydrolysis of collagen. Although gelatine is derived from collagen, it has its own specific properties, which are independent of the properties of collagen. Gelatine should therefor be considered as an individual biomaterial [47].

Gelatine hydrogels can be produced by crosslinking in water above concentration around 2% w/v and below temperatures of 30°C to 35°C. The mechanical properties, such as elasticity, mechanical strength and shape stability, of the gelatine hydrogels diminish at temperatures above these, thus limiting the use of them as biomaterials in vivo [48].

2.7 Scaffold Design and Manufacture

In general there are a few basic requirements that have been accepted for designing polymer scaffolds:

1. A scaffold has to have high porosity and proper pore size.
2. A high surface area is needed.
3. Biodegradability is generally required, and a proper degradation rate is needed to match the rate of neo-tissue formation.
4. The scaffold must have the required mechanical integrity to maintain the predesigned tissue structure.
5. The scaffold should not be toxic to the cells (i.e. biocompatible).
6. The scaffold should positively interact with cells, including enhanced cell adhesion, growth, migration, and differentiated function.

The requirements of biomaterial scaffolds used for tissue-engineered tissue and organ includes three-dimensional scaffold structure, biocompatibility and in most cases biodegradability with a suitable degradation rates. The mechanical strength, porosity, degradation rates, surface chemistry, and incorporation of biologically active molecules all affect the characteristics of the scaffold [49].

When designing a polymeric scaffold three main factors should be taken into account: 1) The architecture of the scaffold, 2) Cell adhesion ligands and 3) Matrix elasticity, as these factors control cell fate.

In this study we are mostly interested in factor 1) and 3), when designing a scaffold for a PUC. The scaffold architecture, such as the fibre size and porosity not only affects the cell adhesion, proliferation and differentiation but also the mechanical properties of the scaffold. Previous studies have shown a remarkable improvement of mechanical properties, when the diameter of polymer fibres is reduced to nano-scale. The surface area to volume ratio, the mechanical properties (such as stiffness and tensile strength) and the flexibility in surface functionalities all increases [50]. The pore size and interconnection between pores affects tissue formation, vascularization, and transportation of nutrients and waste products. An increase in porosity and pore size increases the surface-area-to-volume ratio in the scaffold, which in return gives a larger surface for cell attachment. Polymer fibres enhance cell adhesion due to their excellent surface-area-to-volume ratio, making them a favourable as biomaterial scaffolds [34].

The elasticity of the scaffold influences the cells respond to their environment. To ensure an appropriate cells growth and differentiation, the stiffness of the matrix has to resemble those found in vivo (Figure 2) [51]. The elasticity is very crucial in this study, as the desired scaffold has to be able to provide the same elastic properties as that of the PUC.

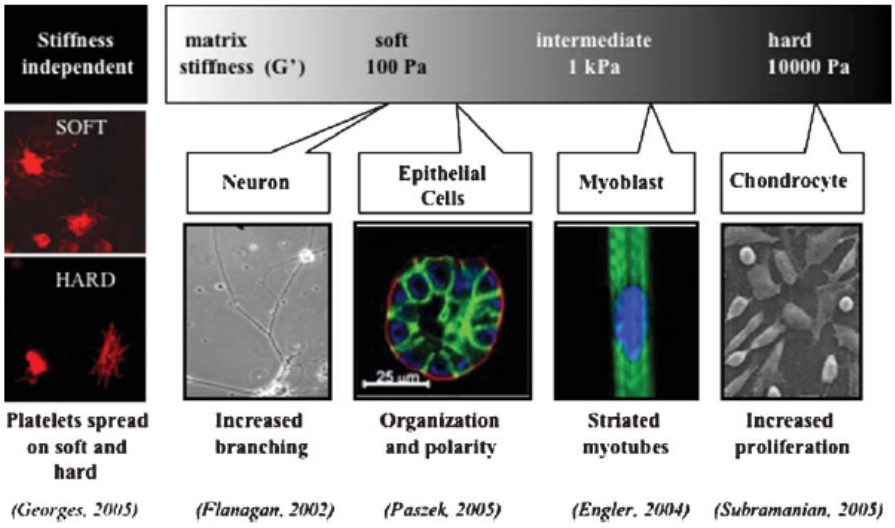

Figure 2. Relationship between matrix stiffness and tissue type [51]

2.7.1 Manufacture of Polymeric Scaffold

Scaffold fabrication techniques affect the properties and functions of a scaffold; hence the choice of fabrication method has to be chosen carefully [34,49]. Several scaffold fabrication techniques have been applied to manufacture polymeric scaffolds including fibre bonding, solvent casting and particulate leaching, and electrospinning.

2.7.1.1 Fibre Bonding

This scaffold fabrication method was initially developed by Mikos et al and involves binding polymer fibres to each other at their intersection points creating a fibre mesh. Mikos et al. used synthetic polymers such as poly(glycolic acid) (PGA) and poly(lactic acid) (PLLA) for their study. The PGA fibres were arranged in a non-woven mesh and exposed to a temperature above the polymers melting point causing the fibres to bond together at their intersection point. The PLLA was dissolved in methylene chloride and casted over the PGA fibre mesh and dried resulting in a PGA-PLLA matrix. The PLLA was removed from the scaffold by dissolving it in

methylene chloride followed by vacuum drying in order to get a pure PGA scaffold [52].

Fibre bonding is a simple scaffold fabrication that provides the ability to maintain the properties of a specific biocompatible polymer. However, the different polymer types that can be used in this fabrication technique are limited and moreover it lacks the ability to control porosity and pore size of the scaffolds [34].

2.7.1.2 Solvent Casting and Particulate Leaching

Solvent casting / particulate leaching is widely used scaffold fabrication method as it allows manufacture of porous scaffolds with controlled porosity (up to 93%), pore diameter (500μm), surface-to-area-volume ratio and crystallinity [34,53,54].

This technique is a process in which applies porogen, such as salt (mostly used), sugar, and wax to create a porous scaffold. The porogen is grounded into small particles with a specific size in order to create the needed porous scaffold. The porogen particles are then poured into a mold and a polymeric solution is casted onto it. The mixture is then evaporated and water is added to remove the porogen particles leaving a polymeric scaffold with desired porosity and pore size. Adjusting the amount and size of the porogen controls the pore size.

Other advantages beside the above mentioned are biocompatibility and the low amount of polymer needed for this fabrication method. However, this method is limited due to its lack of control of pore shape and the interconnected porous network [34].

2.7.1.3 Electrospinning

Electrostatic fibre spinning or electrospinning is a process that produces polymer fibres by forcing an electrical charged jet of polymeric solution. The jet evaporates and the polymer fibres are deposited on a collector [55,56].

This scaffold fabrication method has been used for various biocompatible polymers, such as poly(lactic-co-glycolic acid) (PLGA), Polycaprolactone (PCL), PGA and

Polyurethane with successfully producing polymer fibres between approximately 4-2000 nm in diameter [57].

This technique has been widely used in tissue engineering due to the ability of electrospinning a highly porous (up to 90 %) nano-scaled scaffold and its cost-effectiveness [56,57,58,59]. Although having a low productivity and jet instability, the ability of controlling fibre thickness, scaffold diameter and pore size, makes electrospinning a favourable scaffold fabrication technique in tissue engineering and also the most preferred fabrication method for this study [34].

2.8 Dynamic Mechanical Analysis

Dynamic Mechanical Analysis (DMA) refers to a technique in which a material is subjected to a controlled stress or strain at a constant frequency in a periodic manner. The properties of a DMA can be analysed as the materials response to stress, temperature, and frequency and furthermore be expressed in the terms of dynamic storage and loss moduli and mechanical damping. DMA measures the stiffness, the viscoelastic behaviour and damping of the material.

For viscoelastic materials the stress and the strain are out of phase by the phase angle, δ. This is due to the additional time required for molecular motions and relaxations to occur. The storage modulus, E' , represents the in-phase part of the sinusoidal stress and strain and describes the elastic behaviour of the material, hence the material's ability to store energy and release it after deformation.

The loss modulus, E", represents the "out-phase" part and describes the viscous response of the material. The damping measures the dissipated energy of the material and is represented as tan(δ), which is equivalent to the ratio of the loss and storage modulus. The damping is associated with the material's ability to absorb energy and this changes according to the material's condition, such as its temperature and the applied frequency.

The moduli of different materials can be measured by gradually changing either the frequency or temperature. The glass transition temperature can be detected by carrying out either a temperature or a frequency sweep test, in which the modulus is measured at different temperatures but at a constant frequency or at different frequencies and at a steady temperature.

In the temperature sweep the glass transition temperature can be detected as a large decrease of the storage modulus, as shown in figure 3 [60].

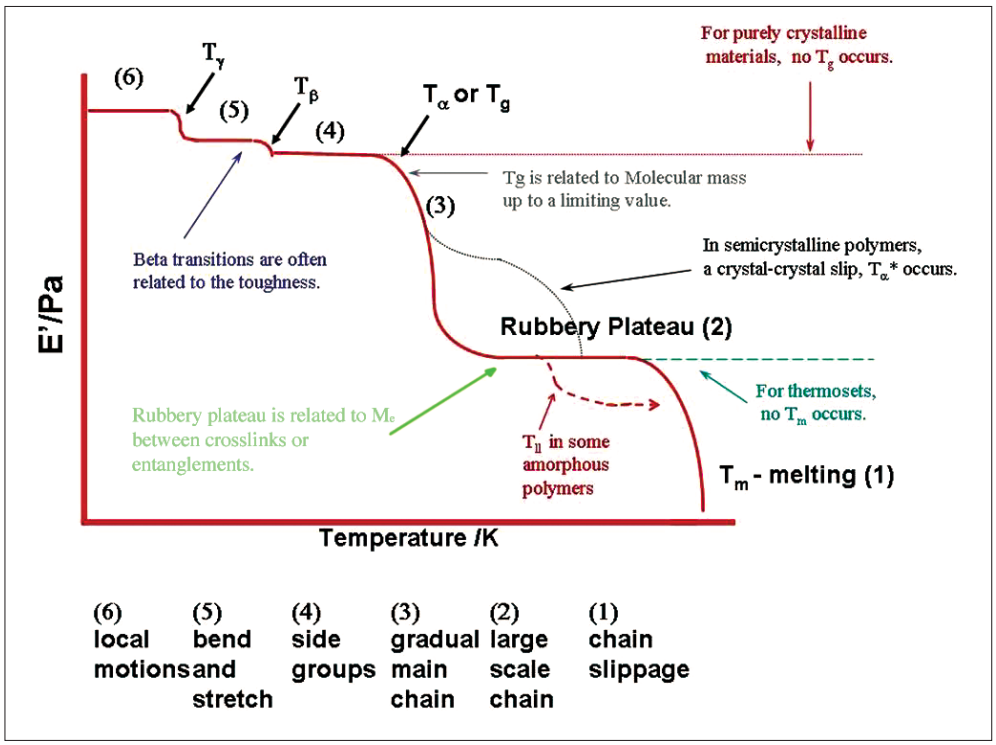

Figure 3. Temperature sweep showing the storage modulus at different temperatures. The glass transition temperature is marked as T_g [73].

3. Project Objectives

The understanding of the mechanical properties of uterine cervical tissue is crucial as these properties can have great impact on the maintenance of a healthy pregnancy and minimise the risk of preterm delivery. The cervix acts as a mechanical barrier holding the foetus in the uterine and as a passage during childbirth. Hence, the mechanical strength of the cervix as well as the elasticity of the tissue are of great interest. For these reasons this project objective was to manufacture biocompatible polyurethane scaffolds with similar mechanical characteristics as those of a PUC.

Polyurethane was chosen due to its biocompatibility in vivo and due to its diverse mechanical properties as this material can be manufactured with different strength and elasticity. The mechanical analysis of the polyurethane scaffolds in the form of nanofibres is crucial in order to understand the effect the scaffolds will have on cell growth and cervical tissue formation. Two different grades of polyurethane were produced and analysed for the scaffold fabrication. The viscoelastic characteristics, elastic moduli, tensile strength, strain and permeability were the main areas of interest.

Previous tissue engineered based studies have shown a relationship between the porosity of scaffolds and the cell growth, survival and differentiation. Therefor this project measured the permeability of the scaffolds in order to evaluate the porosity of the fabricated scaffolds. The mechanical properties of the Z1A1 polymer grade and Z3A1 polymer grade were analysed by using DMA.

Electrospinning was chosen as a nano-scaled scaffold fabrication method due to simple setup of the method, cost-effectiveness and to its ability to electrospin highly porous nano-scaled scaffolds. Scanning microscopy electron (SEM) was used to analyse the morphology of the electrospun scaffolds and fibres.

The scaffold materials were compared before and after impregnation with gelatine, in terms of their viscoelastic behaviour, hydraulic permeability, and fibre morphology,

and with reference to the mechanical properties of the two grades of polymer from which the electrospun forms were made (Z1A1, Z3A1).

4. Materials and Methods

All the equipment used to successfully complete this project were provided by the Department of Biomedical Engineering at the University of Strathclyde.

4.1 POLYMERS

Medical grade polyurethanes Z1A1 and Z3A1 (b9 Series 'A') were supplied under the terms of a Materials Transfer Agreement between Biomer Technology Ltd and the University of Strathclyde for scaffold fabrication. According to the company, these polymers are biocompatible and are compatible with ISO 10993 for biocompatibility. The company further states a wide range of polymer properties, such as low temperature flexibility, a wide dynamic range of hardness and wide range of fabrication techniques. Table 2 shows the company's list of both polymer grades mechanical properties. These values are of great interest for this project as those include high ultimate tensile strength and ultimate elongation and a tensile modulus between 50% and 300%.

Tensile Modulus (MPa)	**Z1A1**	**Z3A1**
50% Elongation	3.1	10.6
100% Elongation	3.9	13.0
200% Elongation	5.8	20.3
300% Elongation	10.9	32.7
Ultimate Tensile Strength (MPa)	39.6	46.7
Ultimate Elongation (%)	555	410

Table 2. The mechanical properties of Z1A1 and Z3A1 provided by Biomer Technology Ltd.

4.1.1 Polymer Solutions

Table 2 gives an overview of the solvent ratios and polymer concentrations applied for the four scaffolds.

Each polymer solution was mixed on a roller for 48 hours at room temperature and atmospheric pressure.

4.1.2 Preparation of the gelatine hydrogels

Gelatine from bovine skin was used to impregnate some of the scaffold samples in order to mimic tissue formation. The gelatine was dissolved in water in room temperature and five petri dish containing gelatine solutions from 1% w/v to 5% w/v were solidified. The solution with 3% w/v of gelatine was chosen due to the texture of the gelatine as concentration below 3% w/v were too soft and more liquidly while the concentrations above were too stiff and solid in order to mimic soft tissue.

4.2 Scaffold Manufacture – Electrospinning

As mentioned above electrospinning was applied as scaffold fabrication method. The electrospinning setup consisted of two Alpha III (Brandenburg, Dudley, UK) high voltage supplies, a metal collector, a syringe pump (PHD 2000, Harvard Apparatus, Kent, UK), and a needle.

The voltage supplies could provide up to 25 kV each to the collector and the shield respectively. The collector was made of stainless metal with a diameter of 4 mm and rotated as the polymer solution moved from the needle towards the collector with a fixed flow rate controlled by the syringe pump.

The electrospinning apparatus was operated according to Standard Operating Procedures (SOP) devised for safe operation (BS EN 61010-1:2010). Safety precautions included cut-off switches and interlocks, and a protective cage to isolate high voltages. To prevent exposure to harmful solvents, the electrospinning process was always carried out in a fume cupboard.

4.2.1 Setup and Process

The electrospinning setup is very simple and consists of a syringe pump with a needle of small diameter, a high voltage source and a collector [56,59]. The syringe pump contains the polymer dispersion and the voltage DC source is applied in order to create a potential difference between the solution and the collector. An electrode is positioned in the solution while another electrode is attached to the collector, which usually is grounded (Figure 4). The syringe containing the polymer solution is exposed to an electric field inducing an electrical charge in the surface of the solution. The solution is retained due to its surface tension. Once the electric field overcomes the surface tension of the solution a jet is ejected from the needle tip and the solution evaporates and polymer fibres are ejected to the collector [56,59].

A stable electrospinning jet consists of four regions; The base region, the jet region, the splaying region, and the collection region.

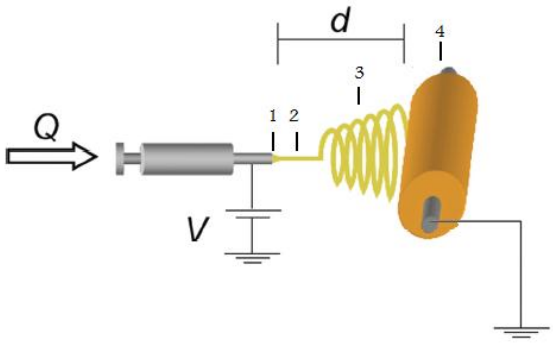

Figure 4. Schematic illustration of electrospinning setup. 1) The base region 2) The jet region 3) the splaying region 4) the collection region. Q=flow rate, d=gap distance and V=Voltage source [59]

4.2.1.1 The Base Region

The intensity of the electric field and the surface tension of the solution cause the solution at the needle tip to elongate and form a conical shape known as the Taylor cone. In the base region the jet is charged and an increase of the electric field produces the ejection of the jet from the tip of the Taylor cone [56,61,62].

4.2.1.2 The Jet Region

As the polymer solution becomes discharged the jet decreases in diameter and undergoes an elongation process. This creates a linear ejection of the jet in the jet region. The decrease in size and elongation of the jet proceeds as the polymer solution evaporates from the base region to the collector [56,61,62]. Charged polymer fibres are produced as the solution evaporates [56].

4.2.1.3 The Splaying Region

Charge repulsion causes the jet to be distributed in many small fibres with roughly same diameter and charge per length. High electric field will lead to instability in the jet causing high frequency oscillation of the jet (Figure 4) [63]. This process occurs several times sequentially, resulting in ejection of a large amount of small charged polymer fibres to the collector. The fibre's thickness can be adjusted by changing the length of the jet [59].

4.2.1.4 The Collection Region

The collection region is where the polymer fibres are collected. The polymer fibres are also influenced by the material type and geometry of the collector. This was confirmed in a previous study, which investigated the collection of PLLA and PLGA polymer, respectively on a metal collector, a water container and a methanol collector. Smoother fibres were collected on the metal collector without complications. Fibres that were collected on the water surface were shrunken, while the methanol collector caused swelling of the fibres [59]. The conductivity of the collector material is important in order to ensure fibres are collected on the collector. Aluminium foil has in previous studies been used due to its high conductivity but a stainless metal rod has been used in this project [25].

4.2.2 Variables of Electrospinning

A range of different parameters can influence the electrospinning process. Dohsi and Reneker have defined these parameters as follow [59]:

- The properties of the polymer solution, such as viscosity, conductivity and the surface tension of the solution.
- Controllable variables, such as the flow rate, the electric field, the distance between the needle tip and the collector, the needle design and size, and the collector material and geometry.
- Ambient variables, such temperature and humidity.

4.2.2.1 Viscosity

The viscosity depends on the concentration of the polymer solution, which in return has an impact on the size and morphology of the electrospun fibres [64,65].

Studies have shown a relationship between low polymer concentrations and beading, which is a process where the fibres are assembled as droplets instead of elctrospun fibres (Figure 5). The concentration of the polymer also affects the diameter of the polymer fibres. Several studies show high polymer concentration increase the fibre diameter [66].

Figure 5. Relationship between beading and viscosity [56]

4.2.2.2 Conductivity and Surface Tension

An increase of the polymer solutions charge density results in uniform polymer fibres and minimises beading [64,65] and is achieved by adding a saline solution to the polymer solution. In order to achieve smoother polymer fibres, alcohol can be added to the solution. Some studies have also shown that by adding alcohol to the polymer solution decrease the surface tension and therefor minimise beading [67].

4.2.2.3 Polymer Flow Rate

Some studies have investigated the relationship between polymer flow rate and the diameter of the polymer fibres and they could conclude that low flow rates reduce the polymer fibres diameter [64] while high flow rates not only result an increase of fibre diameter but also beading [67]. In order to achieve consistent fibres, the flow rate at which the polymer solution is made available for electrospinning should match the rate at which the solution is removed from the needle tip [3].

4.2.2.4 Voltage Density

The potential difference in electrospinning has an impact on the production of the polymer fibres. The intensity of the voltage will affect the fibres diameter as high voltage levels results in faster solvent evaporation and an increase in fibre diameter due to stretching of the fibres. However, this will also increase bead formation, as the droplet at needle tip, forming the Taylor cone will decrease. Low voltage levels increase the volume of the droplet at the needle tip and reduce beads formation but it also results in larger fibre diameter [3,66].

4.2.2.5 Gap Distance

An appropriate distance between the needle tip and the collector has to be set up in order to ensure enough strength of the electric field and sufficient time for the polymer fibres to evaporate before reaching the collector [68]. An increase of the distance leads to a smaller fibre diameters but it can also obstruct the electrospinning process. Further, a reduction of the gap distance can result in wet fibres, as the polymeric solution has insufficient time to evaporate before being deposited onto the collector. This will cause a scaffold with clustered fibres and the fibres tend to stick to the collector and to each other [3].

For some polymer solutions, such as PVA, gelatine, chitosan and poly (vinylidene fluoride) (PVDF), the gap distance has no significant effect on the polymer morphology and fibre size [68,69].

4.2.2.6 Temperature and Humidity

Temperature and humidity can also influence the electrospinning process [70]. A rise in temperature can cause a reduction of the polymer solutions viscosity, which in return causes smaller fibre diameter. An increase of the humidity can result in small circular cracks on the fibre surface [71].

4.2.3 The Scaffolds

Table 3 shows the electrospinning parameters that were chosen for each polymer scaffold.

	Z1A1 Scaffold 1	**Z1A1 Scaffold 2**	**Z3A1 Scaffold 1**	**Z3A1 Scaffold 2**
Flow rate (ml/h)	0.6	0.6	0.3	0.3
Gap distance (cm)	14	14.5	17	13
Voltage supply 1 (kV)*	17	20	17	20
Voltage Supply 2 (kV)**	10	10	10	10
Number of syringes	2	2	2	2
Polymer concentration (% w/w)	6	8	15	15
Solvent	DMF	DMF	DMF and THF	DMF and THF
Solvent ratio (DMF:THF)	100:0	100:0	30:70	60:40
Temperature (°C)	25.1	24.6	26.4	24.7
Humidity (%)	32-35	45-47	31-34	34-47

Table 3. Different electrospinning parameters for each scaffold. * Supplies voltage to the collector. ** Supplies voltage to the shield.

Four tube shaped electrospun scaffolds with a length of 18cm, a diameter of 4mm and a wall thickness ranging between 60μm and 200μm each were produced (Table 3). Two of the scaffolds were made with Z1A1 polymer grade with two different range

of fibre diameter and additional two scaffolds were produced with Z3A1 polymer grade also with different range of fibre diameter.

4.3 Morphology

One main challenge in the electrospinning process was to produce a polymer scaffold with specific fibre diameter while minimising bead formation. The process was prolonged, as finding suitable parameters, such as voltage, gap distance, flow rate and concentration rates were very challenging.

Hitachi TM1000 SEM (Hitachi High-Technologies Europe GmbH, Krefeld, Germany) (Figure 6) was utilised continuously in order to analyse the morphology of the fibres and to detect any occurrence of beading. The SEM has an accelerating voltage at 15kV and a capability to magnify the samples up to 10,000 times with a movement range of 15 x 18 mm.

Figure 6. Hitachi TM1000 SEM

4.4 Permeability Test

A hydraulic permeability test of the scaffolds was performed. This test was chosen, as it would assist the evaluation of the scaffold's porosity.

4.4.1 Sample preparation

Each sample was cut into a 3cm long tube with a diameter of 4mm. Three samples from each polymer scaffold were used for the hydraulic permeability test.

4.4.2 Experiment Setup

A syringe pump (PHD 2000, Harvard Apparatus, Kent, UK) and a BD Plastic 50/60ml syringe containing distillery water were used for controlling the flow rate. The sample was blocked on the distal opening in order to let the water flow through the pores of the sample. A MPC-500 pressure mikro-tip catheter transducer (Millar Instruments, Inc., Houston, USA) was applied to measure the pressure in the sample and the Bose ElectroForce software recorded these values (Figure 7). Each sample underwent five tests three times each with different flow rates of 1ml/min, 2ml/min, 3ml/min, 4ml/min, and 5ml/min.

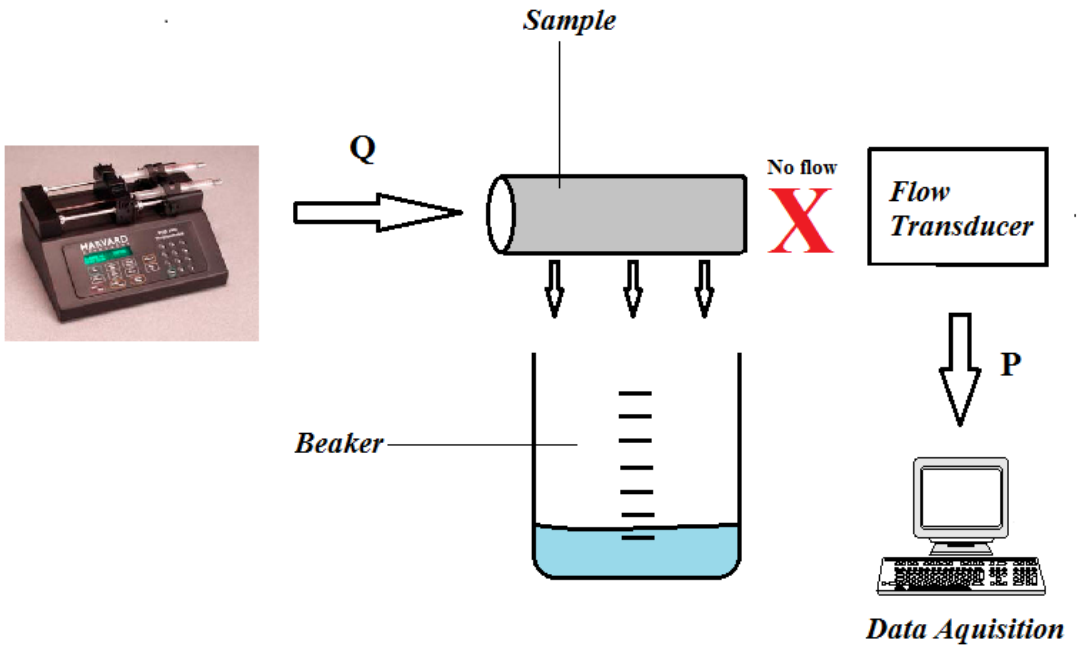

Figure 7. Experiment setup for the permeability test. Q=Flow rate and P=Pressure

4.4.3 Data Acquisition

The pressure inside each sample was recorded every second for 60 seconds and at the five chosen flow rates. The average pressure of each sample at the five flow rates was calculated and these values where used as the pressure value in order to calculate the hydraulic permeability.

The below hydraulic permeability equation was derived from Darcy's law for hydraulic permeability:

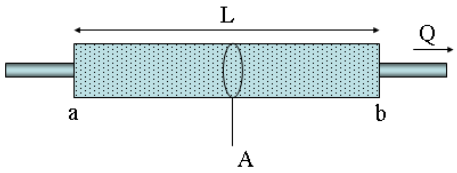

Figure 8. Permeability – Darcy's law

$$Q = \frac{-k \cdot A}{\mu} \cdot \frac{\Delta\rho}{L} \qquad (1)$$

k is the hydraulic permeability

Q is the flow rate of the fluid

$\Delta\rho$ is the pressure drop in the sample

A is the cross-sectional area of the sample

L is the length in which the pressure drop takes place

μ is the viscosity of the fluid

The area of interest in this experiment is the surface area, as the samples used were hollow tubes with pores only in the surface. The length of the pressure drop corresponds to the wall thickness of the samples but as these values were very small and also varied from sample to sample the length was considered negligible.

The fluid used for this test was distilled water at room temperature and as the viscosity of water is approximately 1.0×10^{-3} Pa·s at room temperature this value was insignificant for this experiment.

The hydraulic permeability of the samples is therefor given by:

$$k = \frac{Q}{\rho \cdot A} \qquad (2)$$

k is the hydraulic permeability

Q is the flow rate of the water

ρ is the pressure inside the sample

A is the surface area of the sample:

$A = 2\pi rl$ (3)

r is the radius

l is the length of the sample

4.5 Material Testing

The samples were tested using Bose® Electroforce® (model 3200, Bose Corp., Eden Prairie, MN, USA)

(Figure 9), which is a system used to test the mechanical properties of soft tissues and materials. The Bose system can provide load force up to 225N and a range of grips to hold the samples. Experiments on the system could be performed in air as well as in a variety of liquid at different temperature. However for this project all tests were performed in air and in a distilled water bath at room temperature. The systems associated software allowed to outline different test conditions, such as strain rate, force ramp and displacement. The maximum displacement of the system was 12mm. The software recorded all data and these were saved in a text file. The tests of interest were stress relaxation test and a hysteresis test of the materials, as these tests describes the viscoelasticity of the material. The tests performed were all tensile tests.

Figure 9. Bose ElectroForce 3200 Load Frame System

4.5.1 Sample preparation

For each of the tests, eight samples from each scaffold were used; four longitudinal tube shaped samples with a length of 10mm and a diameter of 4mm and four ring-shaped samples with a width of 3mm and a diameter of 4mm. Half of the samples were impregnated with 3% w/v gelatine solution with a syringe. After some time the gelatine solution solidified to a gel in the pores of the samples.

The gelatine impregnated samples were 48 hours upon testing flushed with distilled water. The protocol used were as follows:

1) The samples were placed in a microwave between 20 and 30 seconds in order to melt the gelatine.
2) The samples were flushed 5 times with distilled water by using a BD 10ml syringe at room temperature
3) Step 1 was repeated
4) Step 2 was repeated
5) Step 1 was repeated
6) Step 2 was repeated
7) The samples were placed in distilled water on a rotator for 1 hour at room temperature
8) The samples were placed in distilled water in a ultrasonic bath for 30 minutes at room temperature
9) All the samples were blow dried with air at room temperature.

The samples without gelatine impregnation also underwent the above protocol. All the samples underwent the same mechanical tests in order to test if there were significantly difference between samples with and without gelatine impregnation.

4.5.2 Stress Relaxation Test

4.5.2.1 Experiment Setup

The longitudinal sample was mounted on two clamps in the Bose system and a force transducer with a maximum force of 450N was applied to measure the load. The sensitivity of the load cell was relatively high, as loads of two decimals could be recorded by the system. The length of the measured area of the samples was 2mm (Figure 10). Three different step strains of 100%, 300%, and 500% were chosen and the sample was exposed to these strains for 60 seconds each without returning the strain to zero in between and the load was recorded by the Bose system.

The same setup was used for the ring-shaped samples although the mounting of the samples was different. The samples were extended along the diameter with two hardened metal hooks mounted to the clamps (Figure 11). The length of the measured area was 4mm, which corresponded to the sample's diameter and they were extended to strains of 50%, 150% and 250%.

All the tests were carried out at room temperature and the samples impregnated with gelatine were submerged in a distilled water bath with room temperature (Figure 12).

The exponential decay at each step strain was applied in order to analyse the stress relaxation rate of each sample type. A slow stress relaxation rate usually indicates that the material has more elastic quality compared to the viscous quality [72].

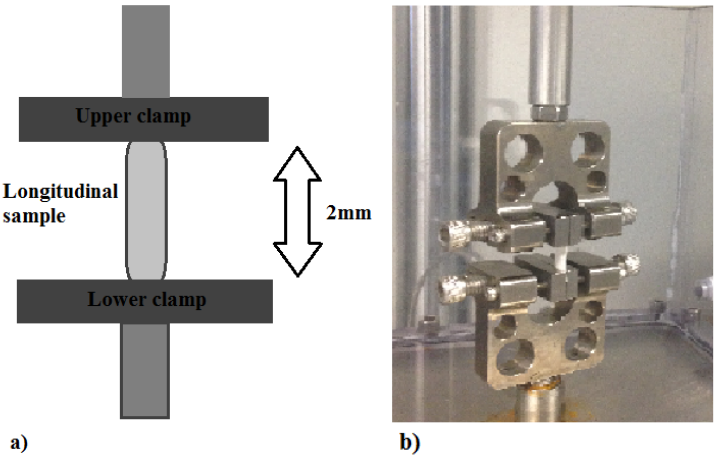

Figure 10. Experiment setup for the stress relaxation test applying longitudinal sample a) schematic illustration of the setup b) The experiment setup

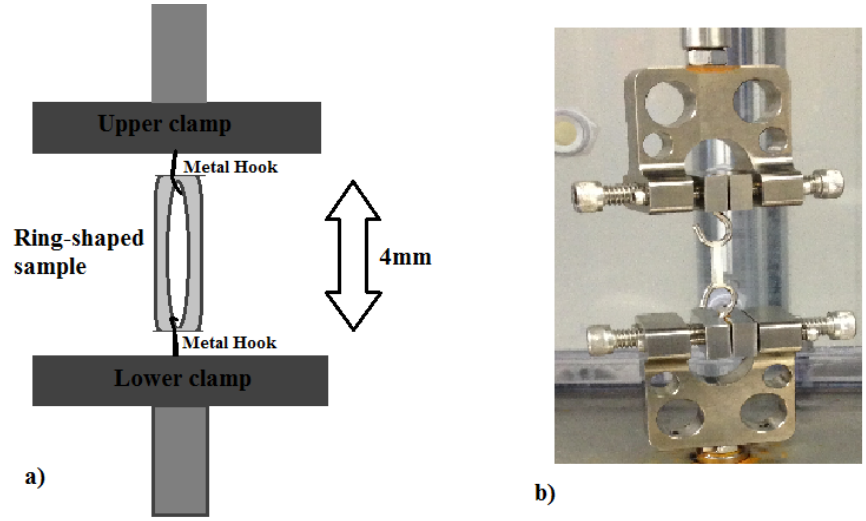

Figure 11. Experiment setup for the stress relaxation test applying ring-shaped sample a) schematic illustration of the setup b) The experiment setup

Figure 12. Experiment setup for the stress relaxation test with distilled water bath.

4.5.2.2 Data Acquisition

The load for each step strain was recorded for each sample. The average loads at different strains were calculated in order to calculate the stress for each sample.

$$\sigma = \frac{F}{A} \quad (4)$$

σ is the stress

F is the measured load

A, for the longitudinal samples, is the surface area of the sample perpendicular to the applied force (Equation (3)) and for the ring-shaped sample the cross-sectional area of the samples were applied:

$$A = \pi \cdot r^2 \quad (5)$$

where r is the radius of the sample

4.5.2.3 Data Analysis

Data was recorded by the Bose system as force (N) and time (s) at three different strains. For the longitudinal samples these strains were 100%, 300%, and 500% while the strains were 50%, 150%, and 250% for the ring-shaped samples.

The recorded forces were thereafter converted to stress (Pa), Eq. 4, and plotted in a graph while disregarding the first second of each test period. This was done in order to retrieve only the exponential function of the stress response and excluding the instantaneous peeks. The anticipated graph for a stress response when a constant strain is applied is as follows for each sample:

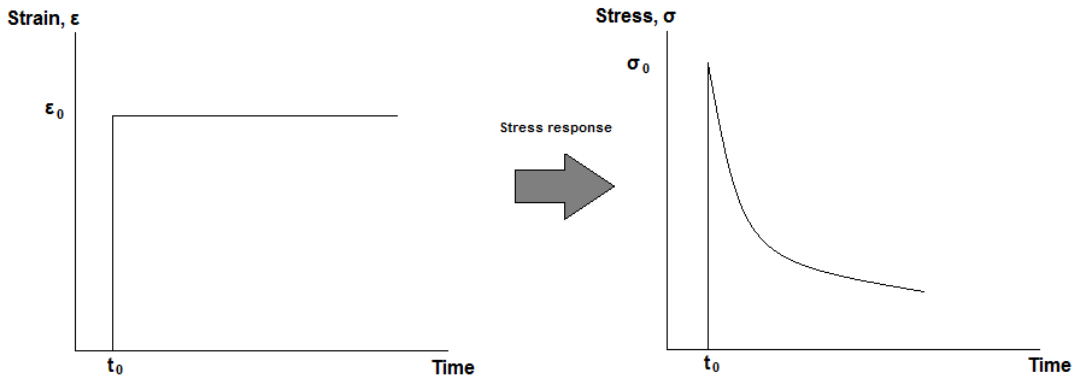

Figure 13. The figure shows the anticipated stress response when a constant strain is applied.

For the comparison of the stress responses of the samples with and without gelatine impregnation the decay constants from the retrieved exponential function was applied for each sample. The decay constants of the four samples without gelatine impregnation were regarded as one group while the decay constants of the remaining two samples with gelatine impregnation were considered as another group.

Two-tailed T-test was applied to calculate the mean and standard deviation of the decay constants for the two groups in order to compare the stress relaxation rate.

Afterwards the decay constants for the Z1A1 samples without gelatine were compared with the Z3A1 samples without gelatine using the same data analyse method as described above.

4.5.3 Hysteresis Test

4.5.3.1 Experiment Setup

The experiment setup for the hysteresis tests was the same as shown in figure 10 for the longitudinal and in figure 11 for the ring-shaped samples. All samples underwent ten loading and unloading cycles. The longitudinal samples first underwent ten loading-unloading cycles with a strain of 100% and additional ten loading-unloading cycles with a strain of 500%. The same was applied for the ring-shaped samples but first with a strain of 50% followed by a strain of 250%. The strain rate was kept

constant at 0.05 mm/s^{-1} and all tests were performed at room temperature. However the samples with gelatine impregnation were submerged in a distilled water bath at room temperature (Figure 12).

4.5.3.2 Data Acquisition

The load and the displacement for each sample were recorded and the stress of each sample was calculated by using equation (4).

The dynamic stress and strain of viscoelastic materials was calculated as follows [75]:

$$\sigma = \sigma_0 \sin(\omega t + \delta) \quad (6)$$

and

$$\varepsilon = \varepsilon_0 \sin(\omega t) \quad (7)$$

ω is the angular frequency and is given by:

$$\omega = 2\pi f \quad (8)$$

f is the frequency and for this experiment this was equal to $\frac{1}{200}$Hz.

δ is the phase lag

The phase lag was found by plotting the strain and stress against the angular frequency ω x time.

Once equation (6) and (7) for stress and strain were plotted in a graph, it was possible to evaluate the viscoelasticity of the material.

The storage and loss modulus, E' and E'', in viscoelastic materials can be expressed as follows:

$$E' = \frac{\sigma_0}{\varepsilon_0}\cos(\delta) \quad (9)$$

and

$$E' = \frac{\sigma_0}{\varepsilon_0}\sin(\delta) \quad (10)$$

4.5.3.3 Data Analysis

Data was recorded by the Bose system as force (N), displacement (mm) and time (s) at three different strains and with ten loading-unloading cycles each. For the longitudinal samples these strains were 100%, 300%, and 500% while the strains were 50%, 150%, and 250% for the ring-shaped samples.

The recorded forces were thereafter converted to stress (Pa) while the displacements were converted to strain but also to elongation (%).

A hysteresis graph with stress against strain was plotted and the anticipated graph after preconditioning was as follows:

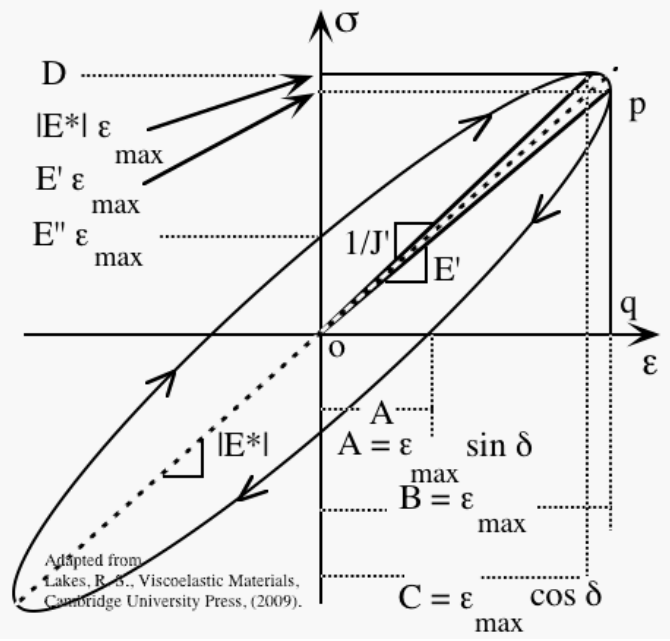

Figure 14. Hysteresis loop of a viscoelastic material. Stress against strain [74]

The phase lag for each sample was read from two sinusoidal wave for stress and strain. The phase lag corresponded to the phase shift between the dynamic stress and strain at the preconditioned state (Figure 15).

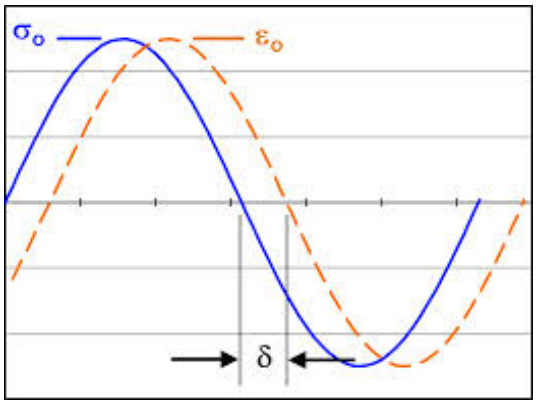

Figure 15. A graph that shows two sinusoidal waves for stress and strain and the phase lag between them.

For the comparison of the viscoelastic properties of the samples with and without gelatine impregnation the phase lag and storage and loss modulus were calculated for each sample. The phase lag and storage and loss modulus of the four samples without gelatine impregnation were regarded as one group while these values of the two samples with gelatine impregnation were regarded as another group.

Two-tailed T-test was applied to calculate the mean and standard deviation of phase lag and storage and loss modulus of the two groups in order to compare the viscoelastic behaviour of the samples with and without gelatine impregnation.

Afterwards the phase lag and storage and loss modulus of the Z1A1 samples without gelatine were compared with the Z3A1 samples without gelatine using the same data analysis method as described above.

5. Results

5.1 Fibre Size

Figure 13 to figure 16 show SEM images of the fibres of the Z1A1 scaffold 1, Z1A1 scaffold 2, Z3A1 scaffold 1, and Z3A1 scaffold 2. All images were scaled by 5000X. The fibre size and wall thickness of the different scaffold is represented in table 4.

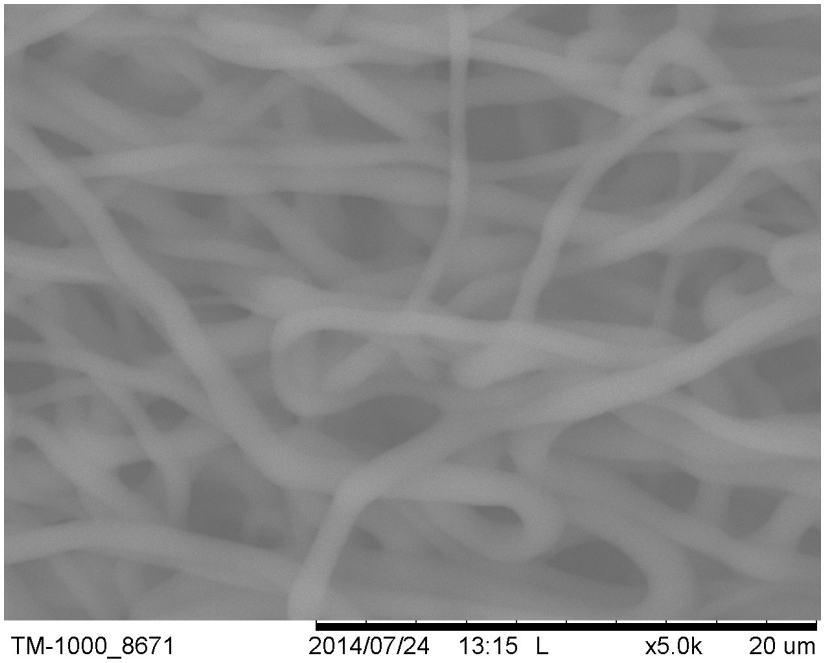

Figure 16. Scanning Electron Microscopy image of the Z1A1 scaffold 1

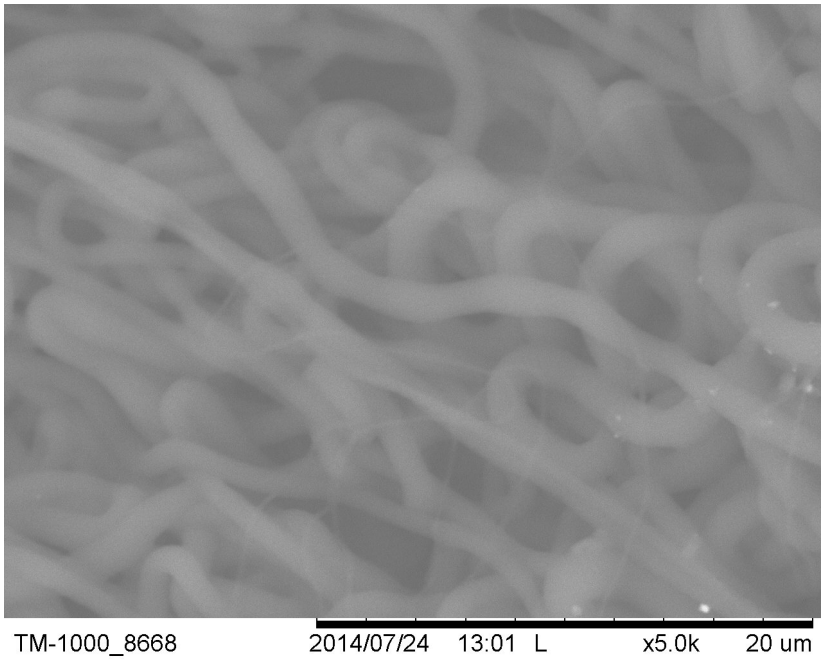

Figure 17. Scanning Electron Microscopy image of the Z1A1 scaffold 2

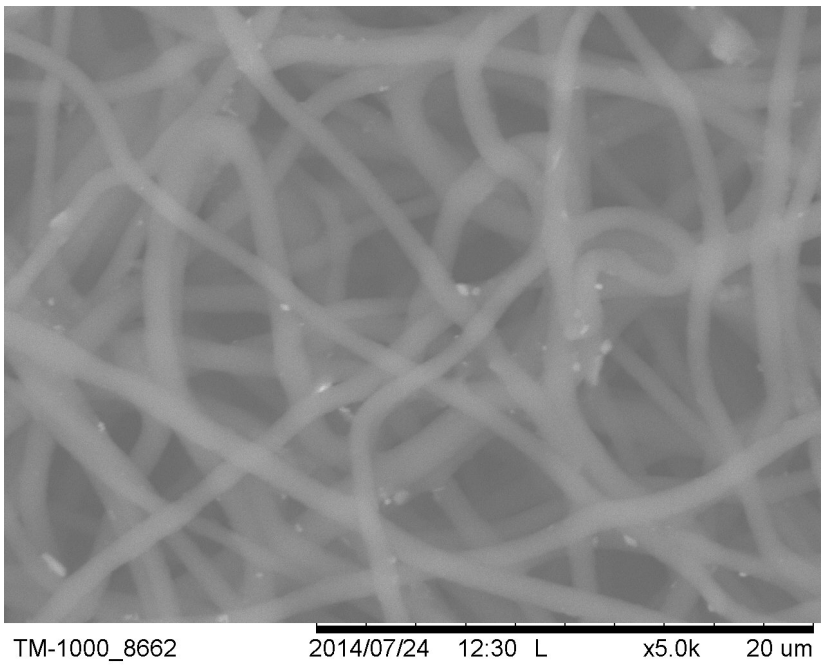

Figure 18. Scanning Electron Microscopy image of the Z3A1 scaffold 1

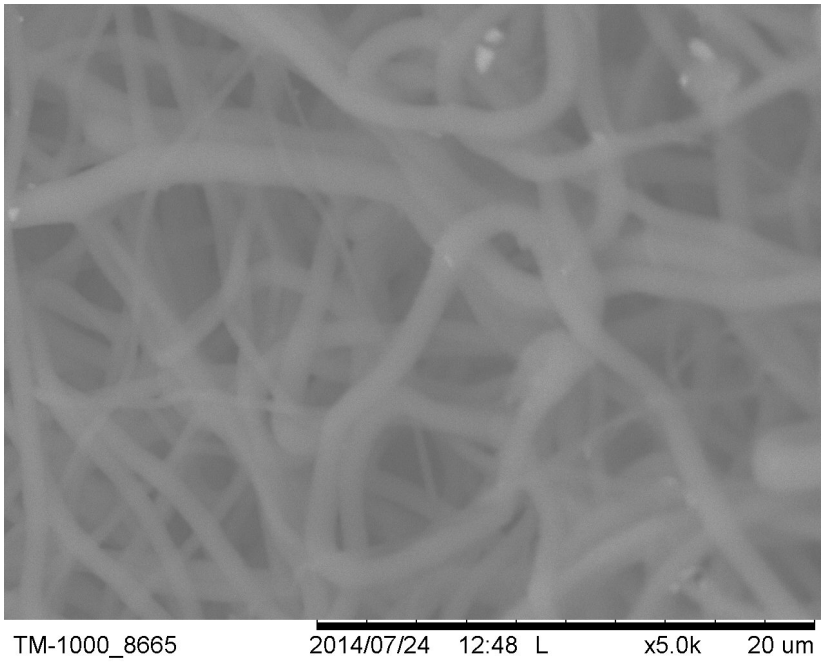

Figure 19. Scanning Electron Microscopy image of the Z3A1 scaffold 2

	Z1A1 Scaffold 1	Z1A1 Scaffold 2	Z3A1 Scaffold 1	Z3A1 Scaffold 2
Length (cm)	18	18	18	18
Diameter (mm)	4	4	4	4
Wall thickness (µm)	60-80	120-130	80-120	120-200
Fibre diameter range (µm)	0.7-1.0	0.5-2.0	0.7-2.0	0.3-2.0
Average Fibre diameter (µm)*	0.49	0.28	0.66	0.50

Table 4. Scaffold dimensions and fibre size. The average is based on the measurements of 10 random fibre diameters from the SEM images (Figure 13 to figure 16).

5.2 Scaffold Permeability

The permeability of all four electorspun scaffolds was tested and the results obtained from the permeability experiments are shown in figure 17 to figure 20. The gradient of the graphs represents the resistance in permeability of each scaffold.

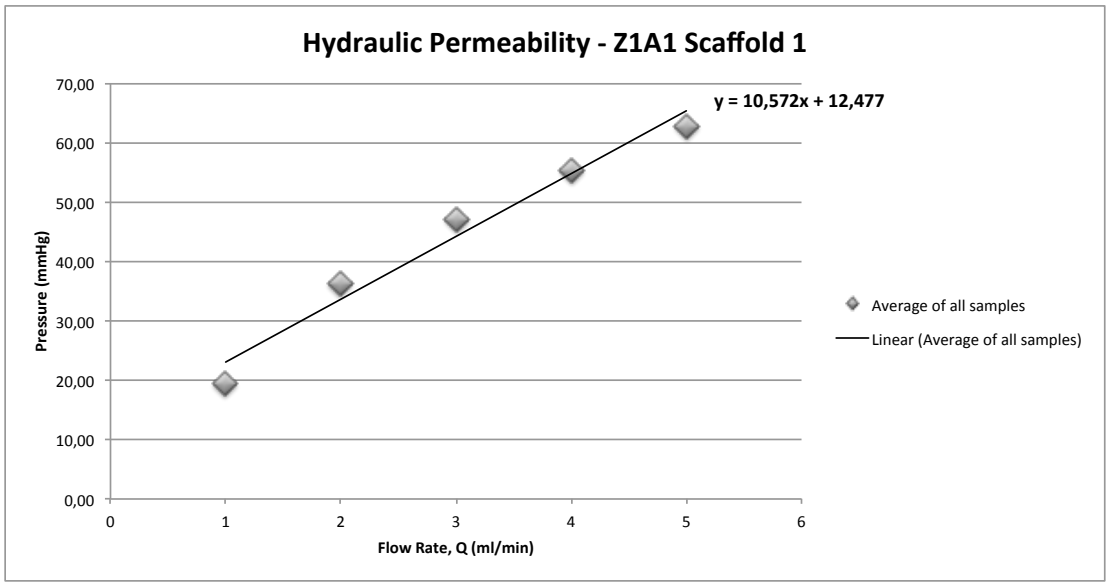

Figure 20. Graph of the hydraulic permeability of the Z1A1 scaffold 1 at five different flow rates (1-5mm/ml)

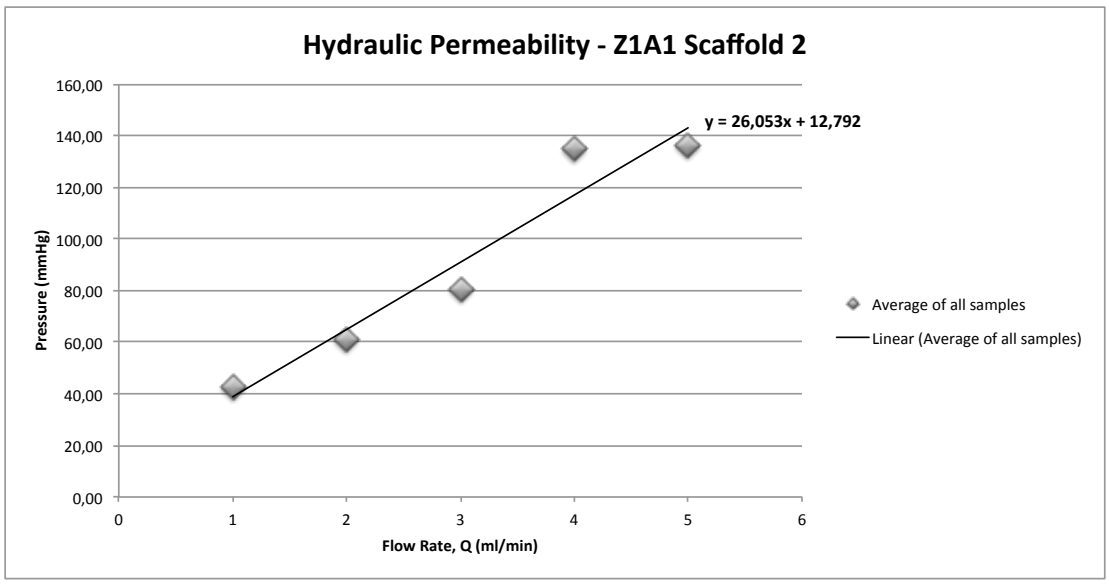

Figure 21. Graph of the hydraulic permeability of the Z1A1 scaffold 2 at five different flow rates (1-5mm/ml)

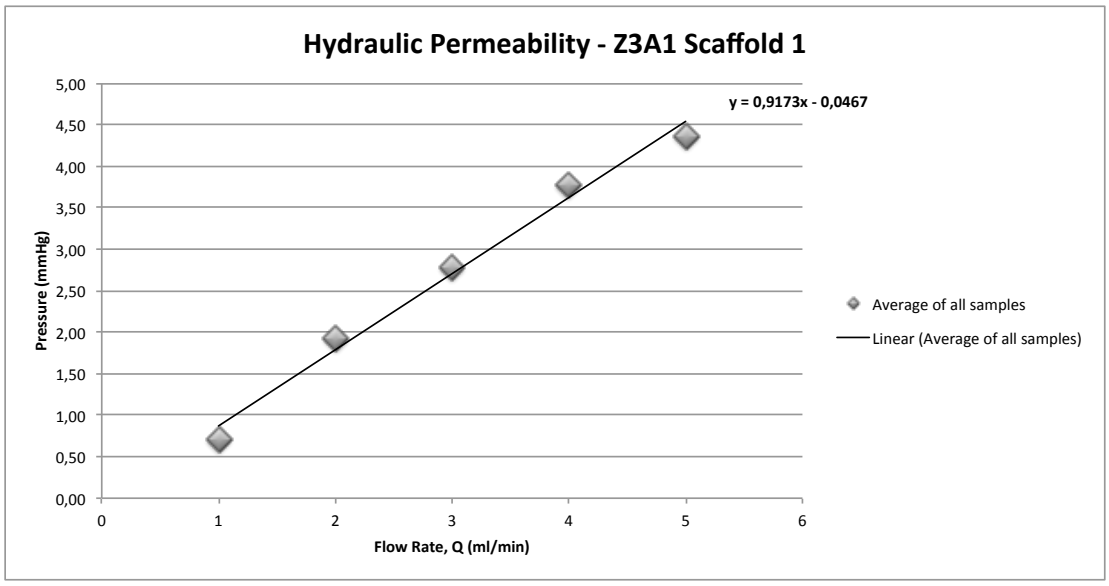

Figure 22. Graph of the hydraulic permeability of the Z3A1 scaffold 1 at five different flow rates (1-5mm/ml)

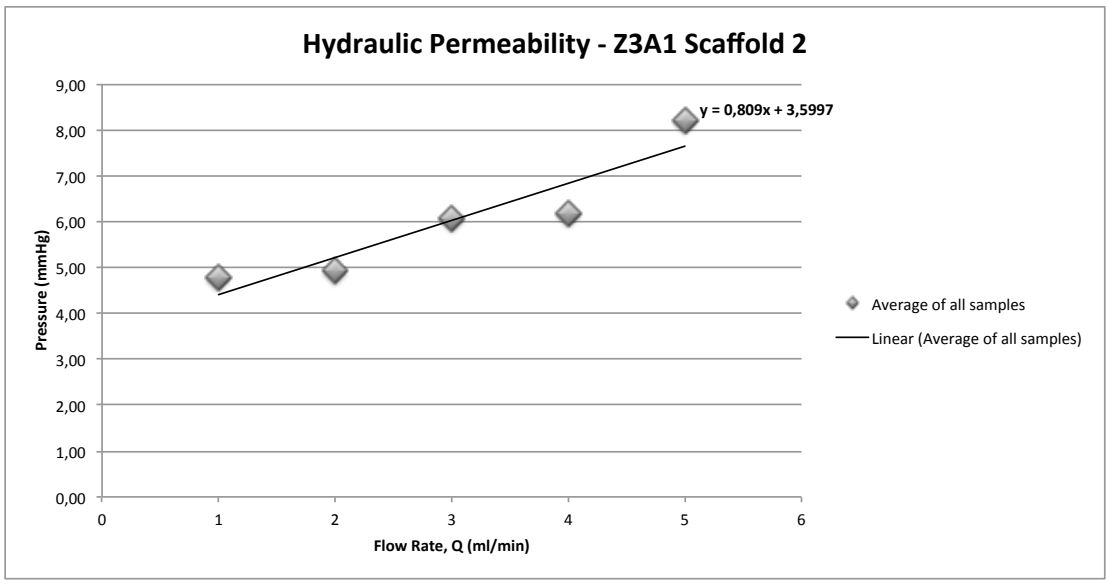

Figure 23. Graph of the hydraulic permeability of the Z3A1 scaffold 2 at five different flow rates (1-5mm/ml)

When the resistance in permeability of the two Z1A1 scaffolds was compared, the resistance was nearly twice as high for the Z1A1 scaffold 2 compared to the Z1A1 scaffold 1.

For the Z3A1 scaffolds the difference in resistance was not as large, however the for Z3A1 scaffold 1 this was slightly higher than for Z3A1 scaffold 2.

In general the resistance in permeability of the Z1A1 scaffolds was much higher than the permeability of the Z3A1 scaffolds.

5.3 Mechanical Properties

The mechanical tests were only performed on the Z1A1 Scaffold 1 and Z3A1 Scaffold 2.

5.3.1 Stress Relaxation

As mentioned earlier different step strains were applied for the longitudinal and ring-shaped samples and these strains were plotted against time, which resulted in exponential graphs. Figure 24 shows an example of these exponential graphs for one Z1A1 longitudinal sample without gelatine impregnation (LS).

The decay constants for these exponential functions were applied in order to analyse the stress relaxation behaviour of the samples.

First the decay constants for the LS/ ring-shaped sample without gelatine impregnation (RS) and longitudinal sample with gelatine impregnation (LSG)/ ring-shaped sample with gelatine impregnation (RSG) were compared and afterwards the decay constants for the Z1A1 and Z3A1 LS/RS samples were compared.

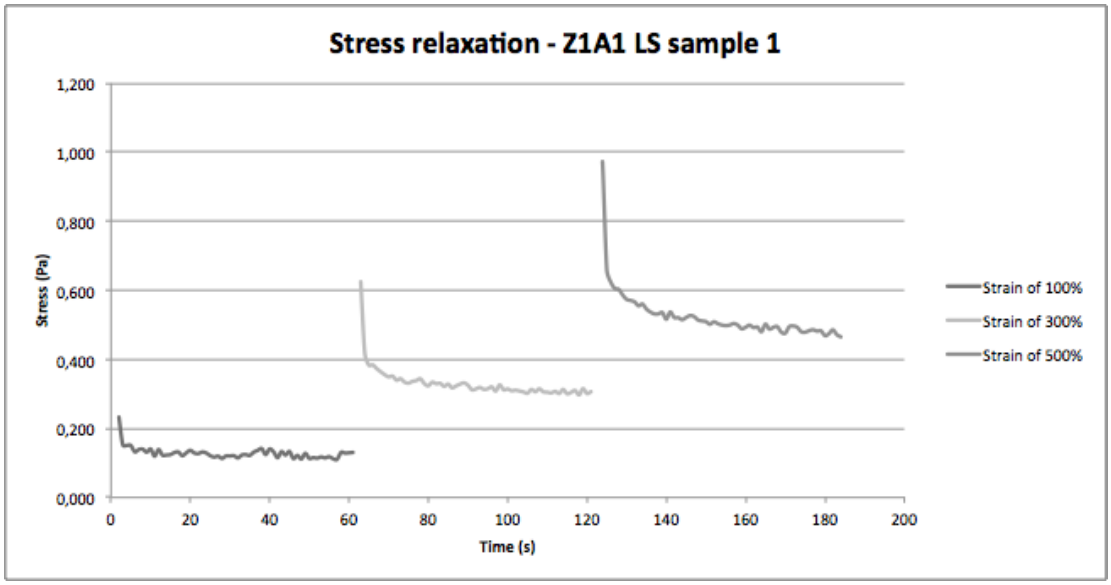

Figure 24. Stress response for Z1A1 LS sample 1 at three different strains of 100%, 300% and 500%

5.3.1.1 Comparison of the stress response of samples with and without gelatine impregnation

5.3.1.1.1 Z1A1 LS and LSG samples

Table 5 shows the mean of the exponential decay constant (λ) for the Z1A1 LS and LSG samples at strain of respectively 100%, 300%, and 500%.

	λ – Strain of 100%		λ – Strain of 300%		λ – Strain of 500%	
Z1A1	Mean	StDev	Mean	StDev	Mean	StDev
LS	-3.0×10^{-3}	1.0×10^{-3}	-4.0×10^{-3}	1.0×10^{-3}	-4.0×10^{-3}	1.0×10^{-3}
LSG	-3.0×10^{-3}	1.0×10^{-3}	-2.0×10^{-3}	0.001	-5.0×10^{-3}	3.0×10^{-3}

Table 5. The mean and standard deviation of the exponential decay constants (λ) of Z1A1 LS and LSG samples at strains of 100%, 300% and 500%.

At elongations of 100% and 300%, the LSG samples relax slower compared to the LS samples. This indicates that LSG samples have more elastic quality compared to the viscous quality. However this changes when the samples are elongated 500% their

original size where the LS samples show a slower stress relaxation compared to the LSG samples.

5.3.1.1.2 Z1A1 RS and RSG samples

Table 6 shows the mean of the decay constant for the Z1A1 RS and RSG samples at strain of respectively 50%, 150%, and 250%.

	λ – Strain of 50%		λ – Strain of 150%		λ – Strain of 250%	
Z1A1	Mean	StDev	Mean	StDev	Mean	StDev
RS	-3.0×10^{-3}	2.0×10^{-3}	-3.0×10^{-3}	1.0×10^{-3}	-3.0×10^{-3}	2.0×10^{-3}
RSG	-2.0×10^{-3}	2.0×10^{-3}	-1.0×10^{-3}	1.0×10^{-3}	-1.0×10^{-3}	1.0×10^{-3}

Table 6. The mean and standard deviation of the decay constants of Z1A1 RS and RSG samples at strains of 50%, 15% and 250%.

The RSG samples relax slower compared to the RS samples at all strain levels. This indicates that RSG samples have more elastic quality compared to the viscous quality.

5.3.1.1.3 Z3A1 LS and LSG samples

Table 7 shows the mean of the decay constant for the Z3A1 LS and LSG samples at strain of respectively 100%, 300%, and 500%.

	λ – Strain of 100%		λ – Strain of 300%		λ – Strain of 500%	
Z3A1	Mean	StDev	Mean	StDev	Mean	StDev
LS	-3.0×10^{-3}	1.0×10^{-3}	-4.0×10^{-3}	5.0×10^{-3}	-4.0×10^{-3}	5.0×10^{-3}
LSG	-5.0×10^{-3}	0.0	-5.0×10^{-3}	0.0	-5.0×10^{-3}	0.0

Table 7. The mean and standard deviation of the decay constants of Z3A1 LS and LSG samples at strains of 100%, 300% and 500%.

The LS samples relax slower compared to the LSG samples at all strain levels. This indicates that LS samples have more elastic quality compared to the viscous quality.

5.3.1.1.4 Z3A1 RS and RSG samples

Table 8 shows the mean of the decay constant for the Z3A1 RS and RSG samples at strain of respectively 50%, 150%, and 250%.

	λ – Strain of 50%		λ – Strain of 150%		λ – Strain of 250%	
Z3A1	Mean	StDev	Mean	StDev	Mean	StDev
RS	-4×10^{-3}	1.0×10^{-3}	-4.0×10^{-3}	1.0×10^{-3}	-5.0×10^{-3}	1.0×10^{-3}
RSG	-4×10^{-7}	0.0	-2.0×10^{-3}	0.0	-3.0×10^{-3}	0.0

Table 8. The mean and standard deviation of the decay constants of Z3A1 RS and RSG samples at strains of 50%, 15% and 250%.

The RSG samples relax slower compared to the RS samples at all strain levels. This indicates that RSG samples have more elastic quality compared to the viscous quality.

5.3.1.2 Comparison of the stress response of Z1A1 and Z3A1 samples

5.3.1.2.1 Z1A1 LS and Z3A1 LS samples

Table 9 shows the mean of the decay constant for the Z1A1 and Z3A1 LS samples at strain of respectively 100%, 300%, and 500%.

	λ – Strain of 100%		λ – Strain of 300%		λ – Strain of 500%	
	Mean	StDev	Mean	StDev	Mean	StDev
Z1A1 LS	-3.0×10^{-3}	1.0×10^{-3}	-4.0×10^{-3}	1.0×10^{-3}	-4.0×10^{-3}	1.0×10^{-3}
Z3A1 LS	-3.0×10^{-3}	1.0×10^{-3}	-4.0×10^{-3}	5.0×10^{-3}	-4.0×10^{-3}	5.0×10^{-3}

Table 9. The mean and standard deviation of the decay constants of Z1A1 and Z3A1 LS samples at strains of 100%, 300% and 500%.

There were no significant differences between the stress responses of the Z1A1 and Z3A1 LS samples.

5.3.1.2.2 Z1A1 RS and Z3A1 RS samples

Table 10 shows the mean of the decay constant for the Z1A1 and Z3A1 RS samples at strain of respectively 50%, 150%, and 250%.

	λ – Strain of 50%		λ – Strain of 150%		λ – Strain of 250%	
	Mean	StDev	Mean	StDev	Mean	StDev
Z1A1 RS	-3.0×10^{-3}	2.0×10^{-3}	-3.0×10^{-3}	1.0×10^{-3}	-3.0×10^{-3}	2.0×10^{-3}
Z3A1 RS	-4.0×10^{-3}	1.0×10^{-3}	-4.0×10^{-3}	1.0×10^{-3}	-5.0×10^{-3}	1.0×10^{-3}

Table 10. The mean and standard deviation of the decay constants of Z1A1 and Z3A1 RS samples at strains of 50%, 150% and 250%.

The Z1A1 RS samples relax slower compared to the Z3A1 RS samples at all strain levels. This indicates that Z1A1 RS samples have more elastic quality compared to the viscous quality.

5.3.2 Hysteresis

Ten loading and unloading cycles were performed on each sample and the samples were all in a preconditioned state after three cycles (Figure 25). First the phase lag, storage and loss moduli of the LS/RS and LSG/RSG samples from each scaffold, Z1A1 and Z3A1, were compared. Furthermore the phase lag, storage and loss moduli of the LS/RS samples from each polymer scaffold were compared.

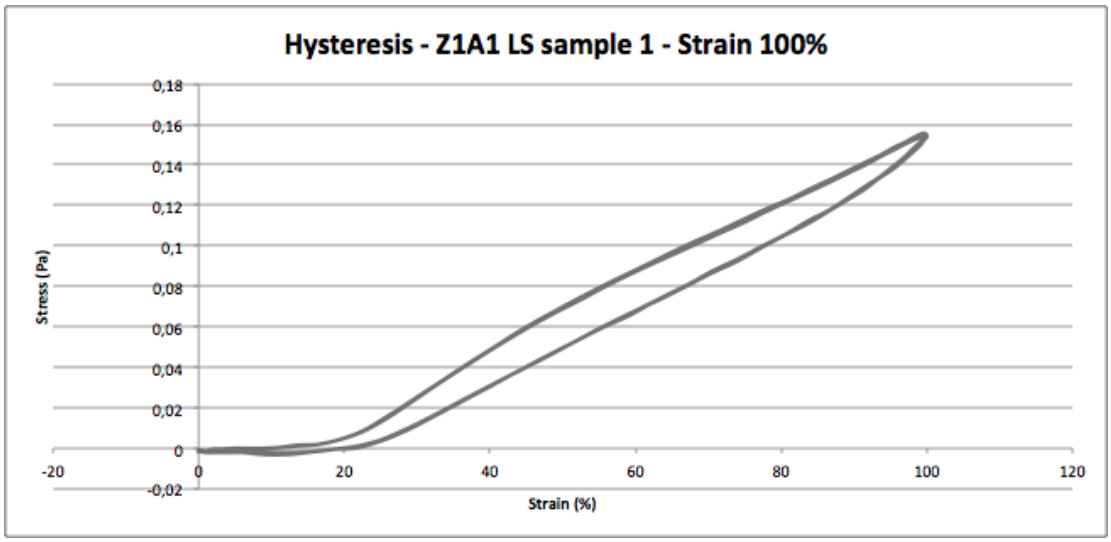

Figure 25. Hysteresis loop for Z1A1 LS sample 1 at a preconditioned state (three last cycles)

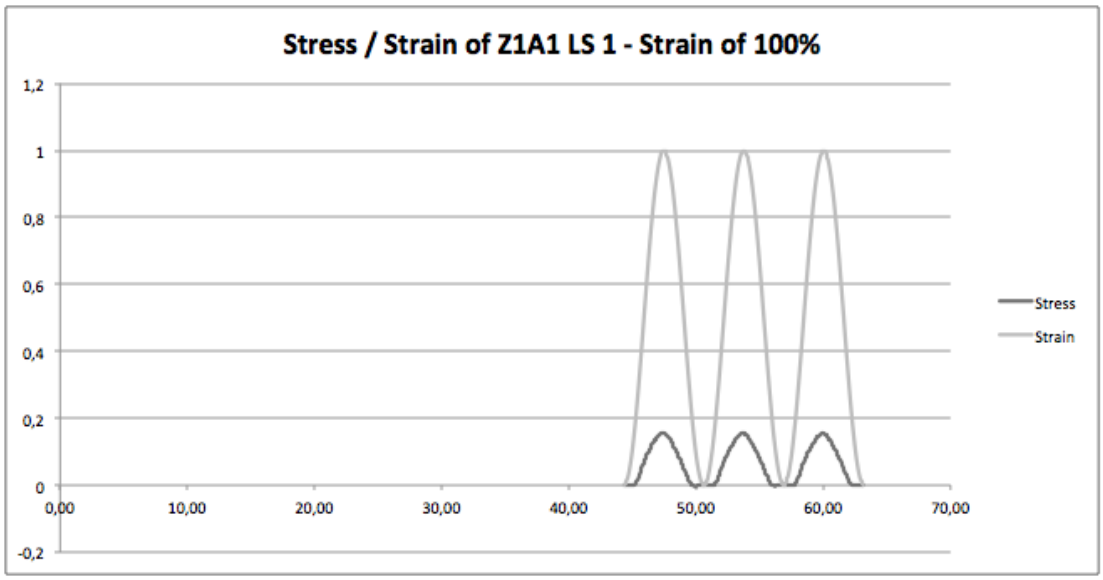

Figure 26. Sinusoidal waves of the stress and strain of Z1A1 LS sample 1 (three last cycles)

5.3.2.1 Comparison between the viscoelastic behaviour of samples with and without gelatine impregnation

5.3.2.1.1 Z1A1 LS and LSG samples

Table 11 and table 12 show the mean of the phase lag and storage and loss modulus for the Z1A1 LS and LSG samples at strain of respectively 100% and 500%.

Z1A1	Phase lag		Storage Modulus, E'		Loss Modulus, E"	
Strain of 100%	Mean	StDev	Mean	StDev	Mean	StDev
LS	390×10^{-3}	60×10^{-3}	920×10^{-3}	30×10^{-3}	390×10^{-3}	60×10^{-3}
LSG	360×10^{-3}	50×10^{-3}	930×10^{-3}	10×10^{-3}	350×10^{-3}	60×10^{-3}

Table 11. Mean and standard deviations values of the phase lag and storage and loss modulus for Z1A1 LS and LSG samples at a strain of 100%

At a strain of 100% there are no significant difference between the storage moduli of the LS and LSG samples. However the LS samples have a higher loss modulus than the LSG samples, which indicates that the LS samples are better in dissipating energy.

Z1A1	δ		E'		E''	
Strain of 500%	Mean	StDev	Mean	StDev	Mean	StDev
LS	530×10^{-3}	120×10^{-3}	850×10^{-3}	60×10^{-3}	500×10^{-3}	110×10^{-3}
LSG	760×10^{-3}	10×10^{-3}	720×10^{-3}	10×10^{-3}	720×10^{-3}	10×10^{-3}

Table 12. Mean and standard deviations values of the phase lag and storage and loss modulus for Z1A1 LS and LSG samples at a strain of 500%

When the strain is increase to 500%, the LS samples show a greater capability of storing energy compared to LSG samples. This indicates that the LS samples are more elastic than the LSG samples when elongated to 500%. Also the loss modulus of the LS samples is lower and again this shows that the LS samples' low ability to dissipate energy compared to the LSG samples.

5.3.2.1.2 Z1A1 RS and RSG samples

Table 13 and table 14 show the mean of the phase lag and storage and loss modulus for the Z1A1 RS and RSG samples at strain of respectively 50% and 250%.

Z1A1	δ		E'		E''	
Strain of 50%	Mean	StDev	Mean	StDev	Mean	StDev
RS	300×10^{-3}	40×10^{-3}	950×10^{-3}	20×10^{-3}	290×10^{-3}	40×10^{-3}
RSG	280×10^{-3}	60×10^{-3}	960×10^{-3}	20×10^{-3}	280×10^{-3}	50×10^{-3}

Table 13. Mean and standard deviations values of the phase lag and storage and loss modulus for Z1A1 RS and RSG samples at a strain of 50%

At a strain of 50% there are no significant difference between the storage and loss moduli of the RS and RSG samples.

Z1A1	δ		E'		E''	
Strain of 250%	Mean	StDev	Mean	StDev	Mean	StDev
RS	630×10^{-3}	140×10^{-3}	800×10^{-3}	80×10^{-3}	580×10^{-3}	120×10^{-3}
RSG	630×10^{-3}	10×10^{-3}	810×10^{-3}	10×10^{-3}	590×10^{-3}	10×10^{-3}

Table 14. Mean and standard deviations values of the phase lag and storage and loss modulus for Z1A1 RS and RSG samples at a strain of 250%

Again at a higher strain of 250% there are no significant difference between the storage and loss moduli of the RS and RSG samples.

5.3.2.1.3 Z3A1 LS and LSG samples

Table 15 and table 16 show the mean of the phase lag and storage and loss modulus for the Z3A1 LS and LSG samples at strain of respectively 100% and 500%.

Z3A1	δ		E'		E''	
Strain of 100%	Mean	StDev	Mean	StDev	Mean	StDev
LS	280×10^{-3}	40×10^{-3}	960×10^{-3}	20×10^{-3}	270×10^{-3}	40×10^{-3}
LSG	320×10^{-3}	220×10^{-3}	990×10^{-3}	10×10^{-3}	310×10^{-3}	210×10^{-3}

Table 15. Mean and standard deviations values of the phase lag and storage and loss modulus for Z3A1 LS and LSG samples at a strain of 100%

At a strain of 100% the storage moduli of the LS samples are lower compared to the LSG samples while the loss moduli for the LS samples are lower. This indicates that the LSG samples are better in storing energy as well as dissipating energy compared to the LS samples.

Z3A1	δ		E'		E''	
Strain of 500%	Mean	StDev	Mean	StDev	Mean	StDev
LS	340×10^{-3}	160×10^{-3}	970×10^{-3}	90×10^{-3}	930×10^{-3}	1220×10^{-3}
LSG	380×10^{-3}	10×10^{-3}	93×10^{-3}	10×10^{-3}	370×10^{-3}	10×10^{-3}

Table 16. Mean and standard deviations values of the phase lag and storage and loss modulus for Z3A1 LS and LSG samples at a strain of 500%

When the strain is increase to 500%, the LS samples show a greater capability of storing energy compared to LSG samples. This indicates that the LS samples are more elastic than the LSG samples when elongated to 500%. However the loss modulus of the LS samples is much higher than the LSG samples.

5.3.2.1.4 Z3A1 RS and RSG samples

Table 17 and table 18 show the mean of the phase lag and storage and loss modulus for the Z1A1 LS and LSG samples at strain of respectively 50% and 250%.

Z3A1	δ		E'		E''	
Strain of 50%	Mean	StDev	Mean	StDev	Mean	StDev
RS	280×10^{-3}	50×10^{-3}	960×10^{-3}	20×10^{-3}	280×10^{-3}	40×10^{-3}
RSG	280×10^{-3}	50×10^{-3}	960×10^{-3}	10×10^{-3}	280×10^{-3}	50×10^{-3}

Table 17. Mean and standard deviations values of the phase lag and storage and loss modulus for Z3A1 RS and RSG samples at a strain of 50%

At a strain of 50% there are no difference between the storage and loss moduli of the RS and RSG samples.

Z3A1	δ		E'		E''	
Strain of 250%	Mean	StDev	Mean	StDev	Mean	StDev
RS	190×10^{-3}	90×10^{-3}	980×10^{-3}	10×10^{-3}	190×10^{-3}	90×10^{-3}
RSG	130×10^{-3}	10×10^{-3}	980×10^{-3}	10×10^{-3}	130×10^{-3}	10×10^{-3}

Table 18. Mean and standard deviations values of the phase lag and storage and loss modulus for Z3A1 RS and RSG samples at a strain of 250%

As the strain was increased to 250% there are still no difference between the storage moduli of the RS and RSG samples. However the loss moduli of the RS samples was higher, which shows that the RS samples are better in dissipating energy compared to RSG samples.

5.3.2.2 Comparison between the viscoelastic behaviour of Z1A1 samples and Z3A1 samples

5.3.2.2.1 Z1A1 LS and Z3A1 LS samples

Table 19 and table 20 show the mean of the phase lag and storage and loss modulus for the Z1A1 and Z3A1 LS samples at strain of respectively 100% and 500%.

	δ		E'		E''	
Strain of 100%	Mean	StDev	Mean	StDev	Mean	StDev
Z1A1 LS	390×10^{-3}	60×10^{-3}	920×10^{-3}	30×10^{-3}	390×10^{-3}	60×10^{-3}
Z3A1 LS	280×10^{-3}	40×10^{-3}	960×10^{-3}	20×10^{-3}	270×10^{-3}	40×10^{-3}

Table 19. Mean and standard deviations values of the phase lag and storage and loss modulus for Z1A1 and Z3A1 LS samples at a strain of 100%

The Z3A1 LS samples have a higher storage modulus compared to the Z1A1 LS samples at strain of 100%. This shows that the Z3A1 are better in storing energy. Nevertheless the Z3A1 LS samples have a lower loss modulus, which shows that these samples are less capable of dissipating energy.

	δ		E'		E''	
Strain of 500%	Mean	StDev	Mean	StDev	Mean	StDev
Z1A1 LS	530×10^{-3}	120×10^{-3}	850×10^{-3}	60×10^{-3}	500×10^{-3}	110×10^{-3}
Z3A1 LS	340×10^{-3}	160×10^{-3}	970×10^{-3}	90×10^{-3}	930×10^{-3}	1220×10^{-3}

Table 20. Mean and standard deviations values of the phase lag and storage and loss modulus for Z1A1 and Z3A1 LS samples at a strain of 500%

The Z3A1 LS samples show to keep having a higher storage modulus compared to the Z1A1 LS samples at strain of 500%, which indicates that the Z3A1 LS samples are better in storing energy. However the Z3A1 LS samples have a higher loss modulus, which shows that these samples are also more capable of dissipating energy.

5.3.2.2.2 Z1A1 RS and Z3A1 RS samples

Table 21 and table 22 show the mean of the phase lag and storage and loss modulus for the Z1A1 and Z3A1 RS samples at strain of respectively 50% and 250%.

	δ		E'		E"	
Strain of 50%	Mean	StDev	Mean	StDev	Mean	StDev
Z1A1 RS	300×10^{-3}	40×10^{-3}	950×10^{-3}	20×10^{-3}	290×10^{-3}	40×10^{-3}
Z3A1 RS	280×10^{-3}	50×10^{-3}	960×10^{-3}	20×10^{-3}	280×10^{-3}	40×10^{-3}

Table 21. Mean and standard deviations values of the phase lag and storage and loss modulus for Z1A1 and Z3A1 RS samples at a strain of 50%

At strain of 50% there are no significant difference between the storage and loss moduli of the Z1A1 and Z3A1 RS samples.

	δ		E'		E"	
Strain of 250%	Mean	StDev	Mean	StDev	Mean	StDev
Z1A1 RS	280×10^{-3}	50×10^{-3}	960×10^{-3}	20×10^{-3}	280×10^{-3}	40×10^{-3}
Z3A1 RS	190×10^{-3}	90×10^{-3}	980×10^{-3}	10×10^{-3}	190×10^{-3}	90×10^{-3}

Table 22. Mean and standard deviations values of the phase lag and storage and loss modulus for Z1A1 and Z3A1 RS samples at a strain of 250%

The Z3A1 RS samples show to have a higher storage modulus compared to the Z1A1 RS samples at strain of 250%, which indicates that the Z3A1 RS samples are better in storing energy. Moreover the Z3A1 RS samples have a lower loss modulus, which shows that these samples are also less capable of dissipating energy.

5.4 Statistic Analysis

5.4.1 Samples used for Permeability Test

ANOVA (Tukey) test was applied in order to find the variation between the three different samples used for each scaffold type and this is illustrated throughout figure 39 to figure 42 showing the mean and standard deviation of each sample.

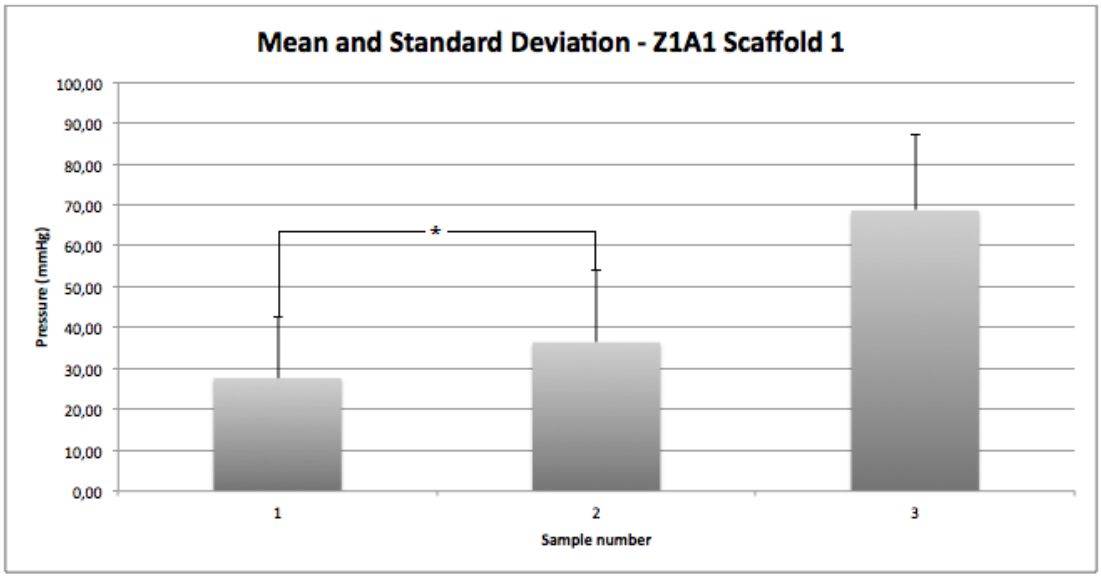

Figure 27. Mean and standard deviation for the three Z1A1 scaffold 1 samples. *There was no significant difference between sample 1 and 2

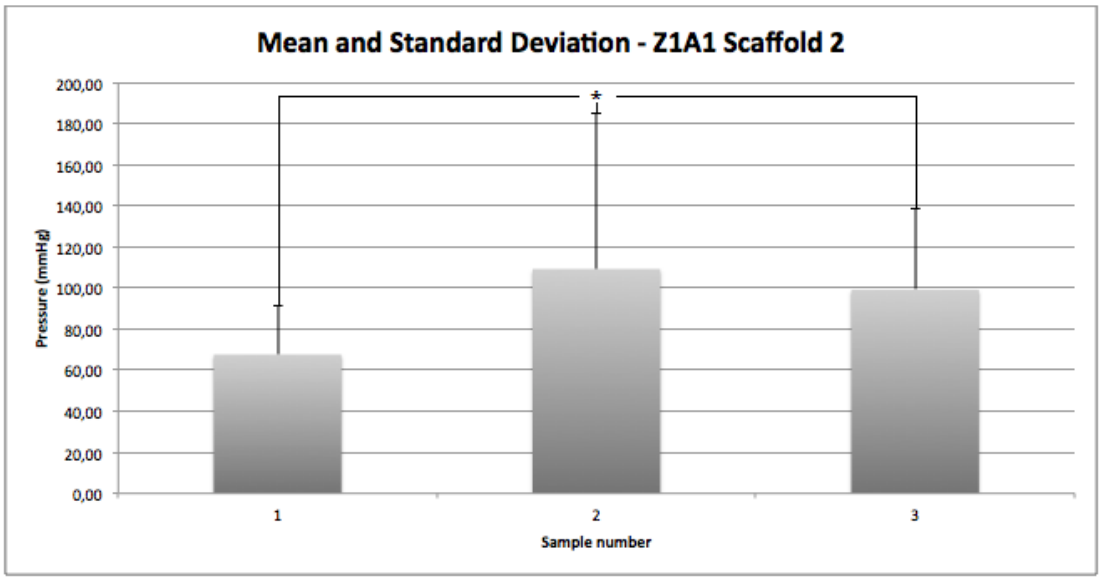

Figure 28. Mean and standard deviation for the three Z1A1 scaffold 2 samples. *There was no significant difference all three samples

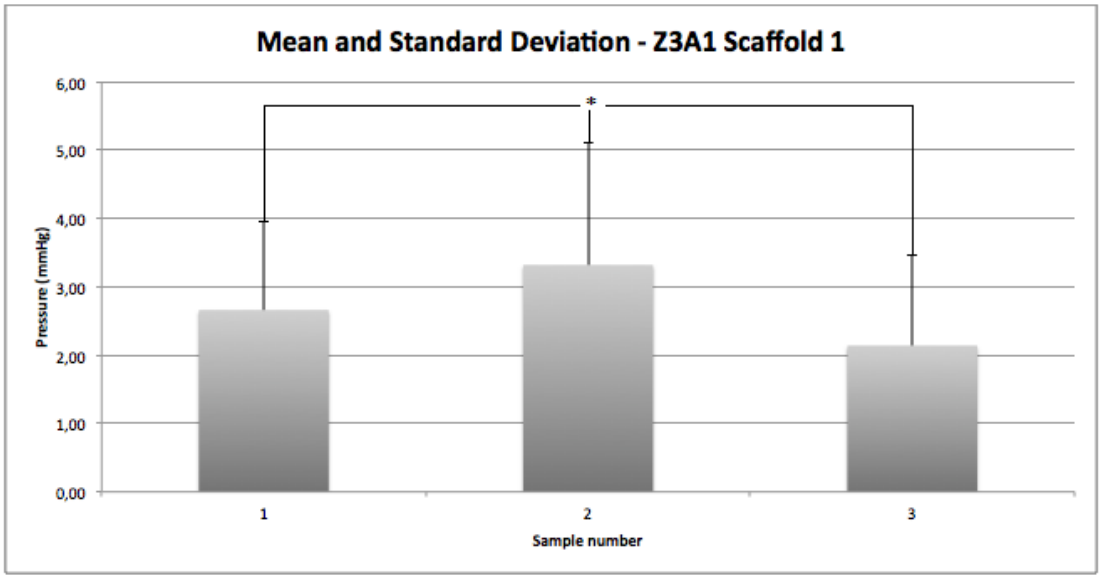

Figure 29. Mean and standard deviation for the three Z3A1 scaffold 1 samples. *There was no significant difference all three samples

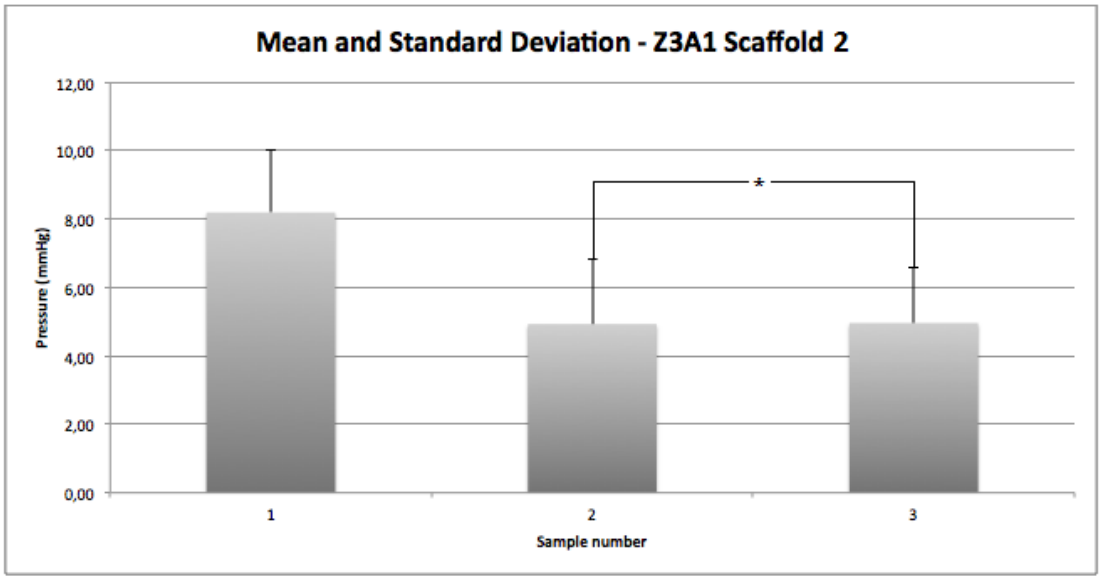

Figure 30. Mean and standard deviation for the three Z3A1 scaffold 2 samples. *There was no significant difference between sample 2 and 3

6. Discussions

Understanding the relationship between the permeability, structure and mechanical properties of the Z1A1 and Z3A1 polymer grade was important in this thesis, as these will give a better understanding of whether or not there are some similarity between these characteristics and those of the UC as well as the usage of these scaffold for tissue engineering a UC in the future.

6.1 Permeability, Fibre Size and Wall Thickness

Investigating the permeability of the scaffolds in this project has been necessary in order to evaluate the porosity of the scaffolds as previous studies have shown a relationship between the porosity and cell proliferation as well as cell differentiation.

The resistance in permeability for Z1A1 scaffold 2 was nearly twice as high as for Z1A1 scaffold 1. In order to study possible causes for this difference, the wall thickness and fibre diameter of the two scaffolds was studied. The larger wall thickness along with small fibre diameter could explain the high resistance in permeability of Z1A1 scaffold 2.

Although the fibre diameters and wall thickness were higher for the Z3A1 scaffolds the hydraulic permeability of the two Z3A1 scaffolds was significantly larger than the Z1A1 scaffolds. However, the SEM images for the Z1A1 scaffolds show more compact fibres compared to the Z3A1 scaffolds and this could be one explanation for the significant difference between the hydraulic permeability of the two polymer scaffolds.

6.2 Viscoelastic Behaviour of the Scaffolds

6.2.1 The Stress Relaxation Test

In order to analyse the viscoelastic behaviour of the scaffolds two tensile mechanical tests were chosen: a stress relaxation test and a hysteresis test.

The step strains that were chosen were a low, medium, and high step strain, as it was important to see if stress relaxation occurred at all three step strain levels. These step strains for the samples were based on the physiological conditions of the UC, as it is known from the literature that the cervix dilates up to 4 times its original size.

For the longitudinal samples a very high step strain of 500% was chosen in order to examine the tensile strength at elongation more than 4 times of the original length.

This was however not possible for the ring-shaped samples since the maximum displacement of the Bose 3200 system was 12mm. The test revealed that both Z1A1 and Z3A1 scaffolds had an instantaneous peak in stress and a prolonged stress relaxation when a step strain was applied. This stress response is well known for viscoelastic materials, which is why this test was chosen as one of the mechanical tests to analyse if the scaffolds exhibited viscoelastic characteristics. The main difference between the samples was observed at step strain of 250% for ring-shaped samples and 500% for longitudinal samples.

The maximum stress response was in general higher for samples with gelatine impregnation, which was anticipated as the purpose of the gelatine impregnation was to mimic tissue growth, which in return would increase the stress.

Another observation was that the stress response was overall higher for the Z3A1 samples compared to the Z1A1 samples. This can be related to the higher tensile modulus and ultimate modulus of the Z3A1 polymer grade and also that Z3A1 contains more of the hard segments compared to Z1A1 polymer grade.

6.2.1.1 Z1A1 LS/RS samples vs LSG/RSG samples

The observed fast stress relaxation of the LSG samples when compared to the LS samples was anticipated as the gelatine impregnation increases the stiffness of the material. However the RSG samples had a slower stress relaxation compared to the RS samples although they were impregnated with the same concentration of gelatine. This difference could have occurred due to less amount of gelatine in these samples, which makes the samples behave like samples without gelatine impregnation.

6.2.1.2 Z3A1 LS/RS samples vs LSG/RSG samples

The stress relaxation rate was almost the same for the LS and LSG samples while it was slightly higher for the RSG samples compared to the RS samples. This small difference could be due to different amount of gelatine impregnated in the longitudinal samples and in the ring-shaped sample.

6.2.1.3 Z1A1 LS/RS samples vs Z3A1 LS/RS samples

The Z3A1 samples exhibited a faster stress relaxation compared to the Z1A1 samples, which shows that the Z3A1 samples revealed to have more of the viscous quality than the elastic quality. This confirms the higher elasticity of the Z1A1 polymer grade compared to the Z3A1 polymer grade.

6.2.2 The Hysteresis Test

Based on the study of Myers et al. [2] a very low strain rate of 0.005mms^{-1} was chosen. This could explain the more elastic characteristic that the samples exhibited during the hysteresis test as the test was pseudo static. The strain rate was however preferred as the UC dilates at low rates during parturition.

The main observation made for the Z1A1 samples and Z3A1 samples was that the Z1A1 samples exhibited a more viscoelastic characteristics than Z3A1 samples,

which showed to be more elastic, as the phase of Z3A1 samples was in general lower than the phase of Z1A1 samples.

During the hysteresis experiments two of the Z3A1 RS samples reached their failure point after two loading-unloading cycles at strain of 500%. Knowing that the Z3A1 polymer grade is stiffer than the Z1A1 polymer grade, one can anticipate the Z3A1 to have a lower failure point than the Z1A1. Nevertheless, the remaining ring-shaped Z3A1 samples were able to undergo all ten loading-unloading cycles without reaching this point, which could be explained as different wall thickness and fibre size of the samples as they were taken from different areas in the 18cm long Z3A1 scaffold 2. It could also be due to defect in the material such as possible cracks on the surface or large internal pores between the fibres resulting in surface cracks.

Another observation that was made was that for samples exposed to a low strain of 100% the Z1A1 LSG samples were more elastic than the LSG samples while this was the opposite for the Z3A1 LS and LSG samples. This indicates that the viscoelastic behaviour of the two polymer grades is different at this strain level.

The difference of storage and loss modulus was not large for LS and LSG samples in general at strain of 100% and this could be do to the low strain rate as well as the low strain of 100%. Most of the LSG samples exhibited a less elastic behaviour when they were exposed to a strain of 500% and this was an anticipated response as polymers exhibit some linear elastic behaviour at lower strains while they are viscoelastic at high strains.

6.3 Alternative Approach

As mentioned earlier a constant low strain rate of 0.005 mms^{-1} was chosen for the hysteresis test, hence a constant frequency. Usually frequency or temperature sweep is applied in DMA in order to analyse the viscoelastic behaviour of materials such as polymers. By gradually changing the frequency or temperature one can find the storage and loss modulus at each frequency or temperature. Therefor an alternative approach for the hysteresis test would be to apply frequency sweep in order to test

any changes in the samples' viscoelastic behaviour, as the strain rate applied for the hysteresis is very low.

It is however important to keep the physiological conditions of the UC, such as the dilation rate, in mind and therefor the frequency range should meet these conditions.

As soft tissue varies in stiffness and texture, a further approach would have been to test the samples with concentration of gelatine, preferably higher than 3% w/v as the gelatine showed to be much softer at concentrations below that.

6.4 Limitations

Scaffolds

The samples used in the stress relaxation and hysteresis test were taken from Z1A1 scaffold 1 and Z3A1 scaffold 2. This was considered as a limitation as it was not possible to evaluate if there was any variations in the mechanical properties if three or more scaffold of each polymer grade was compared.

For the permeability test it was possible to have samples from two Z1A1 scaffolds as well as samples from two Z3A1 scaffolds. However, these scaffolds were electrospun with different parameters even though they were of same polymer grade. This caused the fabrication of different scaffolds in where the fibre diameter, fibre direction and wall thickness varied from scaffold to scaffold (Figure 13 to figure 16).

Elongation limits

The Bose system had an elongation limit of 12mm, which limited the elongation of the ring-shaped samples up to only 250% their original diameter. This limitation of the system also led to the inability to test possible failure point of the samples.

Data and Statistical Analysis

It was not possible to undertake a full statistical analysis of data in all cases owing to the lack of samples and the limited time for research. Therefor the focus was on data retrieved for the LS and LSG samples in the stress relaxation and hysteresis test.

The results for the hysteresis test is based on the data retrieved for the LS and LSG samples only and not for the RS and RSG samples. This was again due to excessive data and limitation of time.

6.5 Further Approach

An analyse of the retrieved data for the RSG samples used in the hysteresis test is needed in order to investigate if there are any resembling between the results of these data and the ones retrieved from the hysteresis test for the LSG samples. This would assist this study to investigate if the material is anisotropic or isotropic.

7. Conclusions

In general the observations made in this project were that mechanical properties, such as the phase lag, phase, storage and loss modulus were not constant for samples with and without gelatine impregnation as well as for Z1A1 and Z3A1 samples.

The permeability of the Z3A1 scaffolds was found to be significantly higher than Z1A1 scaffolds when compared. This indicates that the Z3A1 scaffolds had a higher porosity of than the Z1A1 scaffolds which makes the Z3A1 scaffolds meet one the few basic requirements for designing of polymer scaffolds. Nevertheless, the stress relaxation test showed that a higher stress was needed in order to elongate the Z3A1 samples in air, which indicates that these samples had a lower elasticity compared to Z1A1 samples tested in air. This difference in elasticity was also confirmed in the hysteresis test, which showed that the Z3A1 samples were stiffer when compared to the Z1A1 samples. As elasticity and stiffness of the tissue engineered tissues and organs have a great impact on the cell differentiation, this difference between the Z1A1 and Z3A1 samples should be taken into account when applying Z3A1 scaffolds for a tissue engineered UC in the future.

The results for the gelatine impregnated samples in both the hysteresis test as well as the stress relaxation test showed that there was no consistency in the mechanical properties of the samples when they were compared to the samples without gelatine impregnation and between Z1A1 and Z3A1 impregnated samples. This inconstancy was especially shown when samples were compared at different strain levels.

The constant low strain rate level, hence constant low frequency, chosen for the hysteresis test is suspected to have some influence on the large variation in the results, which it is strongly suggested to perform a frequency sweep test in order to get a broader range of results of the hysteresis test.

7.1 Suggested Future Work

A further study in which the limitations of this project are met is necessarily as these limitations have not been dealt with in this project.

A suggestion for future work is to also perform the stress relaxation and hysteresis experiments, with the limitations taken into account, around 37° instead of room temperature. This is suggested in order to investigate if the mechanical properties of the samples vary significantly from the mechanical properties found in this project, as polymers are sensitive to temperature changes. For the DMA, a temperature sweep test would in this case be preferred.

Besides a tensile mechanical test it is suggested that future work includes compression mechanical tests on the longitudinal samples as compression loads are applied in the longitudinal direction of the UC due to the weight of the foetus.

8. References

1. Shepherd, J. H. (2012). Cervical cancer. *Best Practice & Research Clinical Obstetrics & Gynaecology*, *26*(3), 293-309.
2. Myers, K. M., Paskaleva, A. P., House, M., & Socrate, S. (2008). Mechanical and biochemical properties of human cervical tissue. *Acta Biomaterialia*, *4*(1), 104-116.
3. Bendixen, E., Danielsen, M., Larsen, K., & Bendixen, C. (2010). Advances in porcine genomics and proteomics—a toolbox for developing the pig as a model organism for molecular biomedical research. *Briefings in functional genomics*,*9*(3), 208-219.
4. Orfanoudaki, I. M., Themelis, G., & Koumantakis, E. (2007). *Optical Biopsy of Uterine Cervix Using a Multispectral Imaging Colposcope*. Nova Publishers.
5. Battlehner, C. N., Caldini, E. G., Pereira, J. C. R., Luque, E. H., & Montes, G. S. (2003). How to measure the increase in elastic system fibres in the lamina propria of the uterine cervix of pregnant rats. *Journal of anatomy*, *203*(4), 405-418.
6. Cancer Statistics Registrations, England (Series MB1) , No. 42, 2011
7. Feltovich, H., Hall, T. J., & Berghella, V. (2012). Beyond cervical length: emerging technologies for assessing the pregnant cervix. *American journal of obstetrics and gynecology*, *207*(5), 345-354.
8. To, M. S., Alfirevic, Z., Heath, V. C., Cicero, S., Cacho, A. M., Williamson, P. R., & Nicolaides, K. H. (2004). Cervical cerclage for prevention of preterm delivery in woman with short cervix: randomised controlled trial. *The Lancet*,*363*(9424), 1849-1853.
9. Draper, E. S., Manktelow, B., Field, D. J., & James, D. (1999). Prediction of survival for preterm births by weight and gestational age: retrospective population based study. *Bmj*, *319*(7217), 1093-1097.
10. Petrou, S. (2003). Economic consequences of preterm birth and low birthweight. *BJOG: An International Journal of Obstetrics & Gynaecology*,*110*(s20), 17-23.

11. To, M. S., Alfirevic, Z., Heath, V. C., Cicero, S., Cacho, A. M., Williamson, P. R., & Nicolaides, K. H. (2004). Cervical cerclage for prevention of preterm delivery in woman with short cervix: randomised controlled trial. *The Lancet*,*363*(9424), 1849-1853.
12. Atala, A. (2012). Tissue engineering of reproductive tissues and organs.*Fertility and sterility*, *98*(1), 21-29.
13. Campbell, G. R., Turnbull, G., Xiang, L., Haines, M., Armstrong, S., Rolfe, B. E., & Campbell, J. H. (2008). The peritoneal cavity as a bioreactor for tissue engineering visceral organs: bladder, uterus and vas deferens. *Journal of tissue engineering and regenerative medicine*, *2*(1), 50-60.
14. House, M., Sanchez, C. C., Rice, W. L., Socrate, S., & Kaplan, D. L. (2010). Cervical tissue engineering using silk scaffolds and human cervical cells.*Tissue Engineering Part A*, *16*(6), 2101-2112.
15. Guseva, N. V., Knight, S. T., Whittimore, J. D., & Wyrick, P. B. (2003). Primary cultures of female swine genital epithelial cells in vitro: a new approach for the study of hormonal modulation of Chlamydia infection. *Infection and immunity*, *71*(8), 4700-4710.
16. D'cruz, O. J., Erbeck, D., & Uckun, F. M. (2005). A study of the potential of the pig as a model for the vaginal irritancy of benzalkonium chloride in comparison to the nonirritant microbicide PHI-443 and the spermicide vanadocene dithiocarbamate. *Toxicologic pathology*, *33*(4), 465-476.
17. VODIČKA, P., Smetana, K., DVOŘÁNKOVÁ, B., Emerick, T., Xu, Y. Z., Ourednik, J., ... & Motlík, J. (2005). The miniature pig as an animal model in biomedical research. *Annals of the New York Academy of Sciences*, *1049*(1), 161-171.
18. Mueller, A., Siemer, J., Renner, S., Hoffmann, I., Maltaris, T., Binder, H., ... & Dittrich, R. (2006). Perfused non-pregnant swine uteri: a model for evaluating transport mechanisms to the side bearing the dominant follicle in humans.*Journal of Reproduction and Development*, *52*(5), 617-624.

19. Miessen, K., Sharbati, S., Einspanier, R., & Schoen, J. (2011). Modelling the porcine oviduct epithelium: A polarized in vitro system suitable for long-term cultivation. *Theriogenology*, *76*(5), 900-910.
20. Swindle, M. M., & Smith, A. C. (2008). Swine in biomedical research. In*Sourcebook of Models for Biomedical Research* (pp. 233-239). Humana Press.
21. Kertiles, L. P., & Anderson, L. L. (1979). Effect of relaxin on cervical dilatation, parturition and lactation in the pig. *Biology of reproduction*, *21*(1), 57-68.
22. Healthline BodyMaps. (2005-2014) *Cervix of uterus*. [Online] Available from: http://www.healthline.com/human-body-maps/cervix-uteri#5/12
23. Edström, K. (2009). The porcine cervix. *Epsilon-electronic publishing at the SLU. SLU University Library, St. Louis*, 1-14.
24. Miessen, K., Einspanier, R., & Schoen, J. (2012). Establishment and characterization of a differentiated epithelial cell culture model derived from the porcine cervix uteri. *BMC veterinary research*, *8*(1), 31.
25. Rodríguez-Antolín, J., Nicolás, L., Cuevas, E., Bravo, I., Castelán, F., & Martínez-Gómez, M. (2012). Morphological characteristics of the cervix in domestic sows. *Anatomical science international*, *87*(4), 195-202.
26. Steinbach, J., & Smidt, D. (1970). Cyclical phenomena in the female genital tract of swine—Histological observations. *Journal of animal science*, *30*(4), 573-577.
27. Conrad, J. T., Tokarz, R. D., & Williford, J. F. (1980). Anatomic site and stretch modulus in the human cervix. *Dilatation of the Uterine Cervix: Connective Tissue Biology and Clinical Management*, 255-264.
28. Rechberger, T., Uldbjerg, N., & Oxlund, H. (1988). Connective tissue changes in the cervix during normal pregnancy and pregnancy complicated by cervical incompetence. *Obstetrics & Gynecology*, *71*(4), 563-567.
29. Kamel, R.A., Ong, J.F. Elof Eriksson, E., Junker, J.P.E, Caterson, E.J. (2013). Tissue Engineering of Skin. *American College of Surgeons*. 217 (3), 533-555.
30. Ellis, M., Jarman-Smith, M., & Chaudhuri, J. B. (2005). Bioreactor systems for tissue engineering: a four-dimensional challenge. In *Bioreactors for Tissue Engineering* (pp. 1-18). Springer Netherlands.

31. Metcalfe, A. D., & Ferguson, M. W. (2007). Bioengineering skin using mechanisms of regeneration and repair. *Biomaterials*, *28*(34), 5100-5113.
32. Dhandayuthapani, B., Yoshida, Y., Maekawa, T., & Kumar, D. S. (2011). Polymeric scaffolds in tissue engineering application: a review. *International Journal of Polymer Science*, *2011*.
33. Saltzman, W. M. (2004). *Tissue engineering: engineering principles for the design of replacement organs and tissues*. Oxford University Press, USA.
34. Lanza, R., Langer, R., & Vacanti, J. P. (Eds.). (2011). *Principles of tissue engineering*. Academic press.
35. Rösler, J., Harders, H., & Bäker, M. (2007). *Mechanical behaviour of engineering materials: metals, ceramics, polymers, and composites*. Springer.
36. Ferry, J. D. (1980). *Viscoelastic properties of polymers*. John Wiley & Sons.
37. Kumbar, S., Laurencin, C., & Deng, M. (Eds.). (2014). *Natural and Synthetic Biomedical Polymers*. Newnes, 123-144
38. Nair, L. S., & Laurencin, C. T. (2007). Biodegradable polymers as biomaterials.*Progress in polymer science*, *32*(8), 762-798.
39. Biomaterials and Biocompatibility booklet – Biomedical Engineering Strathclyde University
40. Biomer Technology Ltd., Runcorn, UK
41. Slaughter, B. V., Khurshid, S. S., Fisher, O. Z., Khademhosseini, A., & Peppas, N. A. (2009). Hydrogels in regenerative medicine. *Advanced Materials*,*21*(32-33), 3307-3329.
42. Yaszemski, M. J., Trantolo, D. J., Lewandrowski, K. U., Hasirci, V., Altobelli, D. E., & Wise, D. L. (Eds.). (2003). *Tissue Engineering and novel delivery systems*. CRC Press.
43. Peppas, N. A., Huang, Y., Torres-Lugo, M., Ward, J. H., & Zhang, J. (2000). Physicochemical foundations and structural design of hydrogels in medicine and biology. *Annual review of biomedical engineering*, *2*(1), 9-29.
44. Gil, E. S., & Hudson, S. M. (2004). Stimuli-reponsive polymers and their bioconjugates. *Progress in polymer science*, *29*(12), 1173-1222.

45. Drury, J. L., & Mooney, D. J. (2003). Hydrogels for tissue engineering: scaffold design variables and applications. *Biomaterials*, *24*(24), 4337-4351.
46. Patel, A., Fine, B., Sandig, M., & Mequanint, K. (2006). Elastin biosynthesis: the missing link in tissue-engineered blood vessels. *Cardiovascular research*,*71*(1), 40-49.
47. Murugan, R., & Ramakrishna, S. (2006). Nano-featured scaffolds for tissue engineering: a review of spinning methodologies. *Tissue engineering*, *12*(3), 435-447.
48. Xing, Q., Yates, K., Vogt, C., Qian, Z., Frost, M. C., & Zhao, F. (2014). Increasing mechanical strength of gelatin hydrogels by divalent metal ion removal. *Scientific reports*, *4*.
49. Subia, B., Kundu, J., & Kundu, S. C. (2010). Biomaterial scaffold fabrication techniques for potential tissue engineering applications. *Tissue engineering*,*524*.
50. Huang, Z. M., Zhang, Y. Z., Kotaki, M., & Ramakrishna, S. (2003). A review on polymer nanofibers by electrospinning and their applications in nanocomposites. *Composites science and technology*, *63*(15), 2223-2253.
51. Levental, I., Georges, P. C., & Janmey, P. A. (2007). Soft biological materials and their impact on cell function. *Soft Matter*, *3*(3), 299-306.
52. Mikos, A. G., Bao, Y., Cima, L. G., Ingber, D. E., Vacanti, J. P., & Langer, R. (1993). Preparation of poly (glycolic acid) bonded fiber structures for cell attachment and transplantation. *Journal of biomedical materials research*,*27*(2), 183-189.
53. Ma, P. X., & Langer, R. (1999). Fabrication of biodegradable polymer foams for cell transplantation and tissue engineering. In *Tissue engineering methods and protocols* (pp. 47-56). Humana Press.
54. Lu, L., Peter, S. J., D Lyman, M., Lai, H. L., Leite, S. M., Tamada, J. A., ... & Mikos, A. G. (2000). In vitro and in vivo degradation of porous poly (dl-lactic-co-glycolic acid) foams. *Biomaterials*, *21*(18), 1837-1845.
55. Laco, F., Grant, M. H., & Black, R. A. (2013). Collagen–nanofiber hydrogel composites promote contact guidance of human lymphatic microvascular

endothelial cells and directed capillary tube formation. *Journal of Biomedical Materials Research Part A*, *101*(6), 1787-1799.

56. Huang, Z. M., Zhang, Y. Z., Kotaki, M., & Ramakrishna, S. (2003). A review on polymer nanofibers by electrospinning and their applications in nanocomposites. *Composites science and technology*, *63*(15), 2223-2253.
57. Fujihara, K., Teo, W. E., Lim, T. C., & Ma, Z. (2005). *An introduction to electrospinning and nanofibers* (Vol. 90). Singapore: World Scientific.
58. Fiinzler, A. G., Hafner, J. H., Nikolaev, P., Lou, L., Kim, S. G., Tomanek, D., ... & Smalley, F. E. (1995). Unraveling nanotubes: field emission from an atomic wire.
59. Pham, Q. P., Sharma, U., & Mikos, A. G. (2006). Electrospinning of polymeric nanofibers for tissue engineering applications: a review. *Tissue engineering*,*12*(5), 1197-1211.
60. Menard, K. P. (2008). *Dynamic mechanical analysis: a practical introduction*. CRC press.
61. Reneker, D. H., & Chun, I. (1996). Nanometre diameter fibres of polymer, produced by electrospinning. *Nanotechnology*, *7*(3), 216.
62. Doshi, J., & Reneker, D. H. (1993, October). Electrospinning process and applications of electrospun fibers. In *Industry Applications Society Annual Meeting, 1993., Conference Record of the 1993 IEEE* (pp. 1698-1703). IEEE.
63. Shin, Y. M., Hohman, M. M., Brenner, M. P., & Rutledge, G. C. (2001). Electrospinning: A whipping fluid jet generates submicron polymer fibers.*Applied Physics Letters*, *78*(8), 1149-1151.
64. Zong, X., Kim, K., Fang, D., Ran, S., Hsiao, B. S., & Chu, B. (2002). Structure and process relationship of electrospun bioabsorbable nanofiber membranes.*Polymer*, *43*(16), 4403-4412.
65. Fong, H., Chun, I., & Reneker, D. H. (1999). Beaded nanofibers formed during electrospinning. *Polymer*, *40*(16), 4585-4592.

66. Deitzel, J. M., Kleinmeyer, J., Harris, D., & Beck Tan, N. C. (2001). The effect of processing variables on the morphology of electrospun nanofibers and textiles. *Polymer*, *42*(1), 261-272.
67. Zuo, W., Zhu, M., Yang, W., Yu, H., Chen, Y., & Zhang, Y. (2005). Experimental study on relationship between jet instability and formation of beaded fibers during electrospinning. *Polymer Engineering & Science*, *45*(5), 704-709.
68. Geng, X., Kwon, O. H., & Jang, J. (2005). Electrospinning of chitosan dissolved in concentrated acetic acid solution. *Biomaterials*, *26*(27), 5427-5432.
69. Zhang, C., Yuan, X., Wu, L., Han, Y., & Sheng, J. (2005). Study on morphology of electrospun poly (vinyl alcohol) mats. *European Polymer Journal*, *41*(3), 423-432.
70. Mit-uppatham, C., Nithitanakul, M., & Supaphol, P. (2004). Ultrafine Electrospun Polyamide-6 Fibers: Effect of Solution Conditions on Morphology and Average Fiber Diameter. *Macromolecular Chemistry and Physics*, *205*(17), 2327-2338.
71. Casper, C. L., Stephens, J. S., Tassi, N. G., Chase, D. B., & Rabolt, J. F. (2004). Controlling surface morphology of electrospun polystyrene fibers: effect of humidity and molecular weight in the electrospinning process.*Macromolecules*, *37*(2), 573-578.
72. Brown, R. (Ed.). (1999). *Handbook of polymer testing: physical methods* (Vol. 50). CRC press.
73. Perkin Elmer. (1998-2014) *Dynamic Mechanical Analysis (DMA) – A Beginner's Guide*. [Online] Available from: http://www.perkinelmer.com/CMSResources/Images/44-74546GDE_IntroductionToDMA.pdf
74. Lakes, R. S. (2009). *Viscoelastic materials*. Cambridge University Press. http://silver.neep.wisc.edu/~lakes/VEnotes.html